

DETACHED EDDY SIMULATION OF TURBULENT FLOW ON 2D HYBRID GRIDS

A THESIS SUBMITTED TO
THE GRADUATE SCHOOL OF NATURAL AND APPLIED SCIENCES
OF
MIDDLE EAST TECHNICAL UNIVERSITY

BY

ÖZCAN YIRTICI

IN PARTIAL FULFILLMENT OF THE REQUIREMENTS
FOR
THE DEGREE OF MASTER OF SCIENCE
IN
AEROSPACE ENGINEERING

SEPTEMBER 2012

Approval of the thesis:

DETACHED EDDY SIMULATION OF TURBULENT FLOW ON 2D HYBRID GRIDS

submitted by **ÖZCAN YIRTICI** in partial fulfillment of the requirements for the degree of **Master of Science in Aerospace Engineering Department, Middle East Technical University** by,

Prof. Dr. Canan ÖZGEN
Dean, Graduate School of **Natural and Applied Sciences**

Prof. Dr. Ozan TEKINALP
Head of Department, **Aerospace Engineering**

Assoc. Prof. Dr. Oğuz UZOL
Supervisor, **Aerospace Engineering Department, METU**

Prof. Dr. İsmail H. TUNCER
Co-supervisor, **Aerospace Engineering Department, METU**

Examining Committee Members:

Prof. Dr. Yusuf ÖZYÖRÜK
Aerospace Engineering Dept., METU

Prof. Dr. İsmail H. TUNCER
Aerospace Engineering Dept., METU

Prof. Dr. Haluk AKSEL
Mechanical Engineering Dept., METU

Assoc. Prof. Dr. Oğuz UZOL
Aerospace Engineering Dept., METU

Assoc. Prof. Dr. D. Funda KURTULUŞ
Aerospace Engineering Dept., METU

Date:

I hereby declare that all information in this document has been obtained and presented in accordance with academic rules and ethical conduct. I also declare that, as required by these rules and conduct, I have fully cited and referenced all material and results that are not original to this work.

Name, Last Name: ÖZCAN YIRTICI

Signature :

ABSTRACT

DETACHED EDDY SIMULATION OF TURBULENT FLOW ON 2D HYBRID GRIDS

YIRTICI, Özcan

M.S., Department of Aerospace Engineering

Supervisor : Assoc. Prof. Dr. Oğuz UZOL

Co-Supervisor : Prof. Dr. İsmail H. TUNCER

September 2012, 57 pages

In this thesis study, Detached Eddy Simulation turbulence model is studied in two dimension mainly for flow over single element airfoils in high Reynolds numbers to gain experience with model before applying it to a three dimensional simulations. For this aim, Spalart-Allmaras and standard DES ,DES97, turbulence models are implemented to parallel, viscous, hybrid grid flow solver. The flow solver ,Set2d, is written in FORTRAN language. The Navier-Stokes equations are discretized by first order accurately cell centered finite volume method and solved explicitly by using Runge-Kutta dual time integration technique. Inviscid fluxes are computed using Roe flux difference splitting method. The numerical simulations are performed in parallel environment using domain decomposition and PVM library routines for inter-process communications. To take into account the effect of unsteadiness after the convergence is ensured by local time stepping technique for four order magnitude drop in density residual, global time stepping is applied for 20000 iterations. The solution algorithm is validated against the numerical and experimental studies for single element airfoils in subsonic and transonic flows. It is seen that Spalart-Allmaras and DES97 turbulence models give the same results in the non-separated flows. Grey area is investigated by changing C_{DES} coefficient. Modeled Stress Depletion which cause reduction of eddy viscosity is observed.

Keywords: Turbulence Modeling, Spalart-Allmaras Turbulence Model, Detached Eddy Simulation, Large Eddy Simulation, Finite Volume Method

ÖZ

İKİ BOYUTLU HİBRİD AĞLARDA TÜRBÜLANSLI AKIŞLARIN AYRIK ÇEVİRİTİ BENZETİMİ

YIRTICI, Özcan

Yüksek Lisans, Havacılık ve Uzay Mühendisliği Bölümü

Tez Yöneticisi : Doç. Dr. Oğuz Uzol

Ortak Tez Yöneticisi : Prof. Dr. İsmail H. TUNCER

Eylül 2012, 57 sayfa

Bu tez çalışmasında, ağırlıklı olarak iki boyutta yüksek Reynolds sayısına sahip kanat profili üzerindeki akışlar Ayrık Çevrinti Benzetimi türbülans modeli ile üç boyuta geçmeden önce model hakkında deneyim kazanmak için çalışıldı. Bu amaç doğrultusunda paralel, viskoz, hibrid ağ akış çözücüsüne Spalart-Allmaras ve standart DES ,DES97, türbülans modelleri eklendi. Akış çözücüsü ,Set2d, FORTRAN dilinde yazılmıştır. Navier-Stokes denklemleri hücre merkezli sonlu hacim metodu ile zamanda örtük olarak Runge-Kutta ikili zaman integrasyon metodu kullanılarak çözülmüştür. Ağdasız akılar Roe akı farkı bölme metodu kullanılarak hesaplanmıştır. Sayısal çözümler, çözüm alanının küçük bölümlere ayrılması ve işlemciler arası iletişimin sağlanması için PVM kütüphanesi rutinleri kullanılarak paralel ortamda gerçekleştirilmiştir. Zamana bağımlılığın etkisini hesaba katmak için yerel zaman adımlama tekniği yoğunluk residüsü dört büyüklük derecesi kadar yakınsadıktan sonra, global zaman adımlama tekniği 20000 iterasyon için uygulanmıştır. Çözüm algoritması ses hızı ve altındaki akışlarda sayısal ve deneysel çalışmalarla karşılaştırılmıştır. Ayrışmasız akışlarda Spalart-Allmaras ve DES türbülans modellerinin aynı sonuçları verdiği görülmüştür. C_{DES} katsayısı değiştirilerek Gri alanı araştırılmış ve Çevrinti viskozitesini azaltan Modeled Stress Depletion gözlenmiştir.

Anahtar Kelimeler: Türbülans Benzetimi, Spalart-Allmaras Türbülans Modeli, Ayrık Çevrinti Benzetimi, Büyük Çevrinti Benzetimi, Sonlu Hacim Yöntemi

Dedicated to my parents

ACKNOWLEDGMENTS

I would first like to thank my supervisor Dr. Oğuz Uzol for giving me a chance to study turbulence and its modeling.

I would like to thank my co-adviser Dr. Ismail Tuncer for introducing me CFD with power of parallel computing environment and addressing every question and comment of mine with a perspicacious calm. I attribute the level of my Master degree to him and without him this thesis would not have been completed.

I would thank to my colleagues and staff in the Aerospace Engineering for the use of facility in parallel environment and moral support.

Special thanks go to my friends Emre Yılmaz, Özgür Harputlu, Özgür Tümüklü, Kenan Cengiz, Şahin Coşkun, Armağan Öztürk and Kıvanç Semiz for their moral support during the succesful completion of this thesis.

Finally, I would like to express my sincere thanks to my family for their thrust and support.

TABLE OF CONTENTS

ABSTRACT	iv
ÖZ	vi
ACKNOWLEDGMENTS	ix
TABLE OF CONTENTS	x
LIST OF TABLES	xiii
LIST OF FIGURES	xiv
LIST OF ABBREVIATIONS	xvi
CHAPTERS	
1 INTRODUCTION	1
1.1 Turbulent Flow Prediction	3
1.1.1 Direc Numerical Simulation (DNS)	3
1.1.2 Large Eddy Simulation (LES)	4
1.1.3 Reynolds Averaged Navier-Stokes (RANS) Equations and Closure Models	4
1.1.4 Hybrid Models	4
1.1.4.1 Partially Averaged Navier-Stokes (PANS)	4
1.1.4.2 Hybrid LES-RANS Models (HLR)	5
1.2 Literature Review	6
1.3 Objectives	8
1.4 Thesis Outline	8
2 METHODOLOGY	10
2.1 Navier-Stokes Equations	10
2.2 Turbulence Modeling	12
2.2.1 Spalart-Allmaras Turbulence Model	12

	2.2.1.1	Modeling of the Dynamic Eddy Viscosity . . .	12
	2.2.1.2	Modeling of the Turbulent Production	13
	2.2.1.3	Modeling of the Turbulent Destruction	14
	2.2.2	Detached Eddy Simulation Method	15
	2.2.2.1	Spalart-Allmaras Based DES Model	15
	2.2.3	Grid Generation	16
2.3		Numerical Method	18
	2.3.1	Spatial Discretization	18
	2.3.1.1	Calculation of the Gradients	19
	2.3.2	Temporal Discretization	20
	2.3.2.1	Runge-Kutta Three Stage Method	20
	2.3.3	Parallelization of the Code	21
	2.3.3.1	Partial Virtual Machine	21
	2.3.3.2	Domain Decomposition	22
	2.3.3.3	Parallel Computing Environment	22
	2.3.3.4	Boundary Conditions	22
3		RESULTS AND DISCUSSION	24
	3.1	Validation Case : Transonic Flow Solutions over RAE2822 Airfoil for Steady-State Flow Condition	24
	3.1.1	Effect of Grid Density on the Solution	25
	3.1.2	y^+ Effect on the Solution	27
	3.1.3	Effect of C_{DES} Coefficient on the Solution	29
	3.2	Performance of Parallel Computing	32
	3.3	Flow Solutions Over Aerospatiale Airfoil	33
	3.3.1	Spalart-Allmaras Turbulence Model Solution	35
	3.3.2	DES Turbulence Model Solution	38
	3.4	Flow Solutions Over NACA0015 Airfoil at High Angle of Attack . .	41
	3.4.1	DES Turbulence Model Solution	47
4		CONCLUSIONS	49
	4.1	FUTURE RECOMMENDATIONS	50

REFERENCES	51
----------------------	----

APPENDICES

A Non-Dimensionalization of Governing Equations	55
B Sample Input Data	56
C Mesh File Format	57

LIST OF TABLES

TABLES

Table 1.1	Effects of Turbulent Flows in Engineering Applications. [4]	2
Table 3.1	Free Stream Flow Conditions for RAE2822	25
Table 3.2	Characteristics of Used Grids for Turbulent Flow over RAE2822 Airfoil . .	25
Table 3.3	Computational Details of Used Grids for Turbulent Flow over RAE2822 Airfoil	27
Table 3.4	Y^+ Values of Used Grids for Turbulent Flow over RAE2822 Airfoil	27
Table 3.5	Computational Details of Used Grids for Turbulent Flow over RAE2822 Airfoil	29
Table 3.6	Free Stream Flow Conditions for Aerospatiale Airfoil	33
Table 3.7	Characteristics of Solution Domain for Turbulent Flow Over Aerospatiale Airfoil	33
Table 3.8	Computational Details of Spalart-Allmaras and DES Turbulent Model for Turbulent Flow over Aerospatiale Airfoil	35
Table 3.9	Free Stream Flow Conditions for NACA0015 Airfoil	41
Table 3.10	Characteristics of Used Grids for Turbulent Flow Over NACA0015 Airfoil .	41
Table 3.11	Computational Details of Spalart-Allmaras and DES Turbulent Model for Turbulent Flow over NACA0015 Airfoil	43
Table 3.12	Aerodynamic Coefficients for NACA 0015 Airfoil	44
Table A.1	Non-dimensional Variables.	55

LIST OF FIGURES

FIGURES

Figure 1.1 Turbulence in a Water Jet. [3]	1
Figure 1.2 Three Approach of the Understanding the Turbulence . [5]	2
Figure 1.3 Turbulent Flow Prediction [11]	5
Figure 2.1 Zoomed View of Hybrid-O Grid for Aerospatiale Airfoil	16
Figure 2.2 Zoomed View of Hybrid-C Grid for Aerospatiale Airfoil	17
Figure 2.3 Node and Cell Numbers of Triangular Cells	18
Figure 2.4 A Cell with Its Neighbours	19
Figure 2.5 Sample Domain Decomposition for Aerospatiale Airfoil by Using METIS Software Package (10 partitions)	22
Figure 2.6 Flow Chart of the Parallel Code	23
Figure 3.1 Detailed view of Mesh-440	25
Figure 3.2 Converge History of Different Grids	26
Figure 3.3 Pressure and Skin Friction Coefficient Distrubition	26
Figure 3.4 Converge History of Mesh-440 Solution Domain for Different y^+ Values .	28
Figure 3.5 Pressure and Skin Friction Coefficient Distrubition	28
Figure 3.6 Converge history of Mesh-440 solution domain for different C_{DES} coef- ficient values	29
Figure 3.7 Pressure and Skin Friction Coefficient Distrubition	30
Figure 3.8 Contours of Turbulent Eddy Viscosity of Mesh-440 Solution Domain for Different C_{DES} Coefficient Values	31
Figure 3.9 Speed up factor for the Mesh-440	32

Figure 3.10 Detailed View of Solution Domain for Aerospatiale Airfoil	34
Figure 3.11 Y^+ Distribution over Aerospatiale Airfoil	34
Figure 3.12 Converge History of Residues for Aerospatiale Airfoil	35
Figure 3.13 Pressure Coefficient Distrubition over Aerospatiale Airfoil for Spalart- Allmaras turbulent model	36
Figure 3.14 Skin Friction Coefficient Distrubition over Aerospatiale Airfoil for Spalart- Allmaras turbulent model	36
Figure 3.15 Mach Number and Turbulent Viscosity Ratio Contours for Aerospatiale Airfoil	37
Figure 3.16 Converge History of Residues for Aerospatiale Airfoil	38
Figure 3.17 Pressure Coefficient Distrubition over Aerospatiale Airfoil for DES tur- bulent model	38
Figure 3.18 Skin Friction Coefficient Distrubition over Aerospatiale Airfoil for DES turbulent model	39
Figure 3.19 Mach Number and Turbulent Viscosity Ratio Contours for Aerospatiale Airfoil	40
Figure 3.20 Detailed View of Solution Domain for Naca0015 Airfoil	42
Figure 3.21 Y^+ Distribution over NACA0015 Airfoil	42
Figure 3.22 Converge History of Lift Coefficient for NACA0015 Airfoil	43
Figure 3.23 Converge History of Residues for NACA0015 Airfoil	44
Figure 3.24 Pressure Coefficient Distrubition over NACA 0015 Airfoil for Spalart- Allmaras turbulent model	45
Figure 3.25 Skin Friction Coefficient Distrubition NACA 0015 Airfoil for Spalart-Allmaras turbulent model	45
Figure 3.26 Mach Number and Turbulent Viscosity Ratio Contours for NACA 0015 Airfoil	46
Figure 3.27 Pressure Coefficient Distrubition over NACA 0015 Airfoil for DES turbu- lent model	47
Figure 3.28 Skin Friction Coefficient Distrubition NACA 0015 Airfoil for DES turbulent model	48

LIST OF ABBREVIATIONS

	ACRONYMS	F_v, G_v	Viscous flux vectors
<i>CFD</i>	Computational Fluid Dynamics		GREEK SYMBOLS
<i>CFL</i>	Courant number	α	Angle of attack
<i>DES</i>	Detached Eddy Simulation	$\alpha_1, \alpha_2, \alpha_3$	Stage coefficients in Runge-Kutta time stepping
<i>DNS</i>	Direct Numerical Simulation	μ	Dynamic viscosity
<i>HLR</i>	Hibrid LES-RANS Models	ν	Kinematic viscosity
<i>LES</i>	Large Eddy Simulation	ν_t	Turbulent eddy viscosity
<i>PVM</i>	Partial Virtual Machine	\tilde{v}	Intermediate variable
<i>PANS</i>	Partially Averaged Navier Stokes	ρ	Density
<i>RANS</i>	Reynolds Averaged Navier Stokes	γ	Ratio of specific heats
<i>ZDES</i>	Zonal Detached Eddy Simulation	δ	Thickness of boundary layer
	ROMAN SYMBOLS	Δ	Grid dependent length scale
C_p	Pressure coefficient	Φ	Dummy variable.
C_{DES}	Constant of the DES model	$\tau_{xx}, \tau_{yy}, \tau_{xy}$	Shear stress components.
c	Chord length of the airfoil	Ω_{ij}	Mean rate of rotation tensor.
d	Closest distance to the nearest wall	$ \Omega_{ij} $	Magnitude of vorticity.
e_T	Total energy per unit volume	S_{ij}	Mean strain rate tensor.
\tilde{d}	DES model length scale	$ S_{ij} $	Magnitude of strain.
f_{v1}	Damping function		Subscripts and Superscripts
H	Total enthalpy per unit volume	$()_{ij}$	Coordinate directions
M	Mach Number	$()_t$	turbulence
P_v	Turbulent production	$()^+$	Normalized unit of length
Re	Reynolds number	$()^n$	At n'th step
x, y	Rectangular Cartesian Coordinates		
Y_v	Turbulence destruction		
y^+	Non-dimensional wall distance		
u, v	Cartesian Velocities in x and y directions		
t	Time		
r	Normalized turbulent eddy viscosity		
Q	Vector of conservative variables		
F, G	Flux vectors		

CHAPTER 1

INTRODUCTION

Turbulence can be seen in all around the universe from the flow of the rivers on earth to the cosmic jets in space [1]. Although the exact definition of turbulence still does not come out, Bradshaw, Hinze, T. Von Karman [2] and many other scientists try to give the definition of the turbulence with respect to its characteristics. Some of these characteristics of turbulence are unsteadiness, dissipation, randomness and three dimensionality. Turbulent flows can be two dimensional just in a statistical sense. Basically in turbulence, the flow is consisted of many different length scales vortices called eddies (see Figure 1.1). Large eddies become smaller and smaller until viscous dissipation takes place by giving their kinetic energy. Kolmogorov length scale is the smallest eddy which dies by giving its energy and becomes a part of one large eddy.

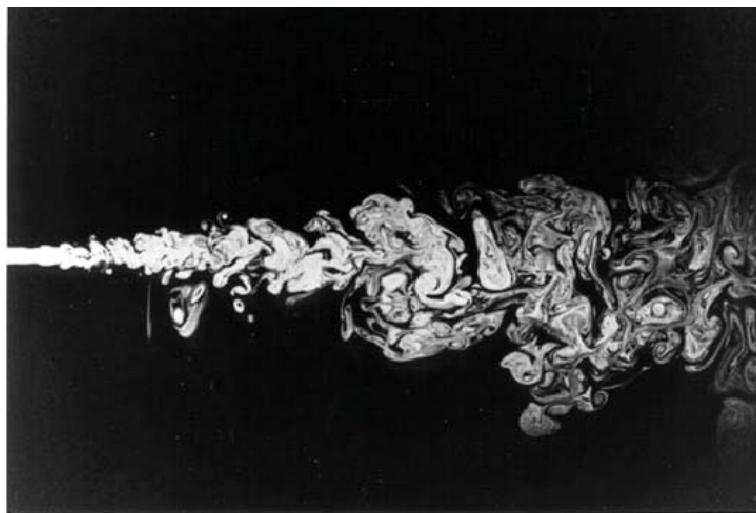


Figure 1.1: Turbulence in a Water Jet. [3]

This process continues until the flow loses turbulent regime. In Aeronautical applications, almost all flow regimes are turbulent and turbulence causes both desirable and unwanted effects on the flows. Some of these effects can be seen in Table 1.1.

Table 1.1: Effects of Turbulent Flows in Engineering Applications. [4]

Advantages	Disadvantages
raised heat, mass and momentum transfer	raised skin friction
rapid mixing	noise production
dissipation of energy	large energy losses

Therefore, engineers and scientist have to predict the turbulent flow. In order to understand and predict the turbulence, there are three approach as worldwide. These are theory, experiment and numerical simulation by computers called Computational Fluid dynamics (usually abbreviated as CFD).

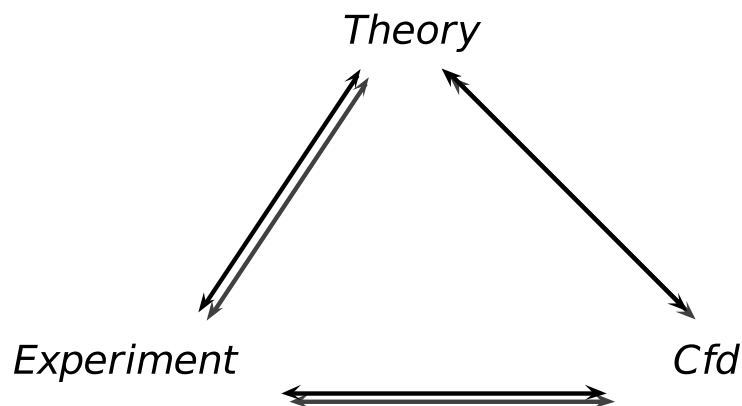


Figure 1.2: Three Approach of the Understanding the Turbulence . [5]

In theory, works on turbulence can be grouped into two part.

1. Understanding Turbulence : several models such as fractals, wavelet, chaos theory.
2. Computing for practical interests : RANS and closure models; LES and derivatives

In the first part, these models just enlarge the vision about homogenous and isotropic turbulence not more. In the second part, all models related to small scale eddies and the effect of

geometrical boundaries where turbulent flow takes place is missed, hence it can be said that these models are useful but incomplete. Detailed explanation can be found in the paper of Çıray C. [6]. Works on turbulence are validated by means of both experiment and CFD.

Turbulent properties such as velocity fluctuations and Reynolds stresses can be measured experimentally by Hot-Wire Anemometer, Particle Image Velocimetry, LDV and others. But since the applicability of the experimental facilities are difficult in most cases: for example, since wind tunnels have many restrictions such as scaling the model and its costliness, the popularity of CFD has increased day by day. In CFD turbulent flows are obtained numerically by solving related partial differential equations. In recent years, it has become possible to solve engineering fluid flow problems using sophisticated numerical methods in supercomputers both in serial and parallel environment.

1.1 Turbulent Flow Prediction

There are many methods for predicting the effect of turbulence with advantages and disadvantages in terms of computational cost and simulation quality. These methods can be grouped into three main and two hybrid categories:

1.1.1 Direct Numerical Simulation (DNS)

Direct numerical simulation (DNS) is the most accurate method within all turbulence modeling methods. In this method, time dependent Navier-Stokes equations are solved and all the relevant time and length scales of turbulence are resolved directly without any turbulence model for the flow considered with appropriate initial and boundary conditions. Since the numerical methods merely affect the accuracy of the solution, it yields detailed information about turbulence properties, which can be difficult to obtain even in experiments. Although DNS is the best way for obtaining turbulent flow solution, computational cost increases with respect to Reynolds number so rapidly (Re^3) and DNS grids must be fine enough to resolve the smallest scale eddies. Therefore, it is just applicable to the simple engineering applications at low Reynolds numbers nowadays by computer power.

1.1.2 Large Eddy Simulation (LES)

In the Large Eddy simulation (LES), the governing equations are spatially filtered to separate the large scale eddies from small scale eddies depending on the mesh size. While large scale eddies are resolved like in DNS, small scale eddies are modelled by subgrid scale (SGS) models. The main challenge to practical use of LES on engineering applications is fine mesh resolution which is comparable with DNS near the wall boundaries.

1.1.3 Reynolds Averaged Navier-Stokes (RANS) Equations and Closure Models

In Reynolds Averaged Navier-Stokes equations, governing equations is decomposed into mean and fluctuating quantities. After this decomposition, an extra term which is called Reynolds stress tensor comes out and the impact of this tensor is modeled with eddy viscosity based closure models. There are many closure approaches available ranging from simple algebraic models to second order closure models. Detailed description of these RANS closure models can be seen in Hoffmann [7], Wilcox [8] and Pope's [9] books. Turbulent prediction of the most of the engineering applications are obtained from solution of RANS.

1.1.4 Hybrid Models

The main purpose of hybrid methods are to combine RANS turbulence models with DNS/LES for obtaining more accurate results in affordable computational cost. Basically in the hybrid models, RANS with one of the closure approaches is used near the wall boundaries to reduce mesh intensity of the grid and DNS/LES is used at the rest of the domain. If DNS is to be used, the hybrid model is called Partially Averaged Navier-Stokes (PANS) model otherwise, it is called hybrid LES-RANS model.

1.1.4.1 Partially Averaged Navier-Stokes (PANS)

Partially Averaged Navier-Stokes turbulence model unite the advantage of RANS and DNS. In this method, filter width can be in any breadth from RANS to DNS scale. In order to derive the PANS equations from the parent RANS equations, appropriate filter width is identified with control parameters. PANS equations solve unresolved kinetic energy and dissipation.

Therefore, one can decide how much of the kinetic energy and dissipation rate is to be modeled. Sharath S. Girimaji described the PANS hybrid turbulence model in detail [10] .

1.1.4.2 Hybrid LES-RANS Models (HLR)

Hybrid LES-RANS models combine Reynolds Averaged Navier-Stokes and Large Eddy Simulation to take advantage of both techniques. In order to reduce the computational cost, RANS is used near the walls and remaining regions is solved by LES. This method is generally referred to as Detached Eddy Simulation (DES) in literature but there are also new versions of DES to overcome grey area problem. These new hybrid models are obtained by modifying DES. Some of them are ; Delayed detached eddy simulation (DDES) and Zonal detached eddy simulation (ZDES) methods. More information about these new models can be found in references of [22, 23, 24].

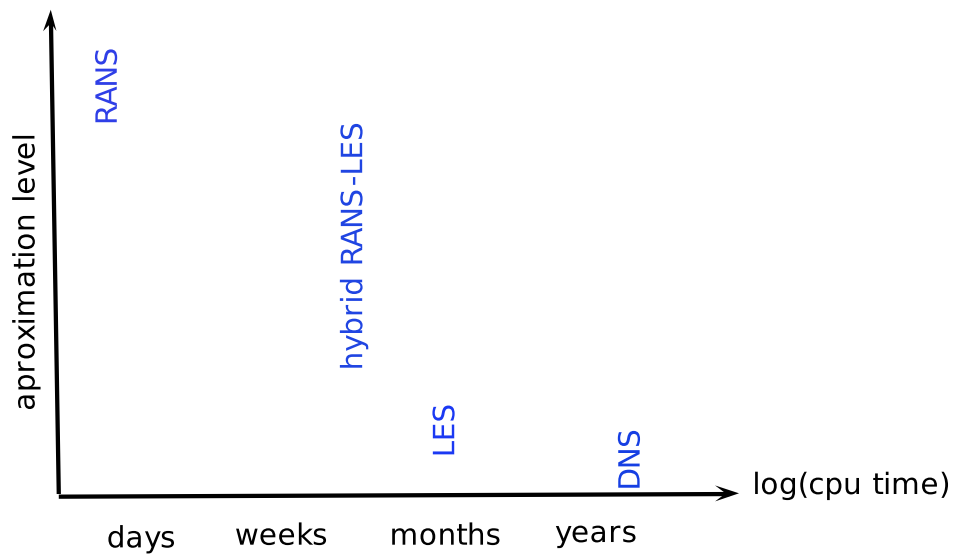


Figure 1.3: Turbulent Flow Prediction [11]

Figure 1.3 gives an general idea about turbulence modeling in the 3D engineering applications. It can be seen that time consuming changes from days to year. The user must choose appropriate model for his/her case.

1.2 Literature Review

Flat plate, turbulent channel flow, backward facing step flow, turbulent flow over an airfoil and cylinder are extensively used to validate the turbulence models. In this part, literature review of numerical studies with Detached-Eddy Simulation turbulence model is given.

For the first time in 1999, DES is used by Shur et al [17] to simulate flow over the NACA0012 airfoil at high angle of attack. They used Spalart-Allmaras as a RANS turbulence model and obtained good results in 3D with experimental data. Benezza et al [20] performed flow over an elliptic airfoil at chord Reynolds number of 7.21×10^6 using 2D DES turbulence model. They investigated C_L and C_D for various values of angle of attack. They compared their results with experimental data and 2D Spalart-Allmaras turbulence model results. Although 2D DES failed to predict the stall, better result from Spalart-Allmaras and good agreement with experimental data were obtained. Kunz et al [21] experinced DES based on $k - \epsilon$ turbulence model on cavitation flow over a hydrofil at angle of attack of 7° . They performed both 2D and 3D simulations for different cavitation numbers.

Bozinovski and Davis [19] implemented DES to their $k - \omega$ RANS turbulence model and tried out on the NACA0012 airfoil at highly seperated flow. They found that while 3D DES gives the best result with experimental data, 2D DES over-predict the C_L and C_D but gives more accurate results than RANS. They attributed the problem in 2D DES to under prediction of the diffusion term since the interaction of eddies in the third dimension were not taken into account.

Flow over a circular cylinder is studied extensively both in low and high Reynolds numbers. Some of the DES applications in circular cylinder can be found in [26, 27, 28] for assessment and comparison.

Breuer et al. [37] simulated flow over a inclined flat plate ($Re=20000$ and $\alpha = 18^\circ$) to compare and evaluate RANS, DES and LES using the same spatial and temporal discretization in Finite Volume Method. Their computations were performed in the same block structured grids with different grid resolutions. They observed that the RANS model was not able to capture the unsteady vortex shedding and although DES computations were not able to reproduce Kelvin-Helmholtz instability sufficiently, DES based on the Spalart-Allmaras turbulence model was successful.

Gilling et al. [38] studied the effect of inflow turbulence on the flow over NACA 0015 in subsonic flows. DES simulation was performed at Reynolds number of 1.6×10^6 for various angle of attack. They found that, especially, close to the stall free stream, turbulence influenced the flow.

Dong Li [39] studied airfoil stall characteristics numerically using standard DES and Baldwin-Lomax based DES turbulence models. He predicted leading edge, trailing edge and thin airfoil stall at Reynolds numbers of 5.8×10^6 and Mach number of 0.3. This study indicated that DES approach can handle massively separated flows and determine stall aerodynamical characteristics of airfoils.

Madsen et al. [40] investigated the performance of DES on thick airfoils at a Reynolds number of 6×10^6 . The 30% thick DU-97-W-300 and the 35% thick DU-97-W-351 airfoils were chosen to see the capabilities of the 3D DES. When they compared their DES result with experimental data, poor agreement near the separated region was observed. This discrepancy was due to high dependency in the transition location and they suggested to use fine mesh and small step size on thick airfoils.

Tu et al. [34] implemented Spalart-Allmaras based DES turbulence model to the hybrid finite volume/element solver. In this solver while the momentum equations were solved with the matrix-free implicit cell centered finite volume method, the pressure Poisson equation was solved by node based Galerkin finite element method. When they performed simulations in high Reynolds number, instability problem was encountered inside the boundary layer. Some modifications were applied on damping functions of Spalart-Allmaras turbulence model to improve robustness.

Aerospatiale single element airfoil was studied extensively especially in highly separated flow by large groups within EU projects. The experimental data for various angle of attack was performed by ONERA in wind tunnel and LES [35], DES, RANS [36, 41, 42, 43] turbulence models were experienced.

In his review paper, Spalart [25] summarized the history, current status and perspectives of DES. Mockett [29] carried out DES turbulence model for a wide range of test cases. In his thesis, he investigated the performance of DES turbulence model in more detail.

To perform RANS-LES methods in engineering applications, especially for European Aero-

nautics Industry, FLOMANIA [30] and DESider [31] projects were put into practice by means of the European-Union Funded Projects. Many organisations from academic institutions to partners from industry were involved in this two projects and obtained results published in [32] and [33].

1.3 Objectives

Set2D is a two-dimensional, parallel cell centered finite volume laminar flow solver which employs upwind flux differencing schemes such as Steger-Warming flux vector splitting, Roe and HLLC for convective fluxes and three stage Runge-Kutta scheme for time integrating. Set2d uses dual time stepping technique for steady/unsteady flow simulations. The computational grid is partitioned by METIS and parallelization is done by using Parallel Virtual Machine libraries.

The aim of this study is to get knowledge about parallel computing, simulate turbulent flows and, by using standard DES turbulence model, gain experience on it. For this purpose, Spalart-Allmaras and DES turbulence models are implemented into Set2D Navier-Stokes solver. The effects of grid density, C_{DES} coefficient and y^+ value are investigated.

1.4 Thesis Outline

In Chapter 2, information about turbulence modeling, grid generation and parallelization is given in detail. Besides, numerical methodology related with finite volume method and turbulence modeling is explained.

In Chapter 3, the numerical results of single element airfoils obtained by Set2d are demonstrated and discussed. Firstly, the effects of grid density resolution, y^+ value and C_{DES} coefficient on solution are studied on Transonic RAE2822 airfoil in steady state mode. In addition, parallel performance of the code is analyzed with respect to the speed up. Then, unsteady flow over Aerospatiale and NACA0015 airfoils are predicted by using Spalart-Allmaras and DES turbulence models. Obtained solutions are compared with the commercial CFD code Fluent results, experimental data and other computational studies.

Chapter 4 gives the conclusion about the study and states suggestions for the future work about this work.

CHAPTER 2

METHODOLOGY

2.1 Navier-Stokes Equations

Because instantaneous values and quantities obey to the Navier-Stokes equations, turbulence is identified mathematically by these partial equations. Navier-Stokes equations depict the conservation of mass and momentum equations. Density, total energy of the fluid and components of the momentum flux can be obtained by solving concurrently the Navier-Stokes equations [12]. The integral compact form of the non-dimensionalized conservation form of governing equations for incompressible flow with no external body force written in 2-D in cartesian coordiante system is as follows :

$$\frac{\partial}{\partial t} \int_{\Omega} Q dx dy + \oint_S (F dy - G dx) = \oint_S (F_v dy - G_v dx) \quad (2.1)$$

where Q is the vector of conservative variables, F and G are flux vectors, F_v and G_v are viscous flux vectors.

$$Q = \begin{bmatrix} \rho \\ \rho u \\ \rho v \\ \rho e_T \end{bmatrix} \quad (2.2)$$

$$F = \begin{bmatrix} \rho u \\ \rho u^2 + p \\ \rho uv \\ \rho uH \end{bmatrix} \quad \text{and} \quad G = \begin{bmatrix} \rho v \\ \rho uv \\ \rho v^2 + p \\ \rho vH \end{bmatrix} \quad (2.3)$$

$$F_v = \begin{bmatrix} 0 \\ \tau_{xx} \\ \tau_{yx} \\ \tau_{xx}u + \tau_{xy}v \end{bmatrix} \quad \text{and} \quad G_v = \begin{bmatrix} 0 \\ \tau_{xy} \\ \tau_{yy} \\ \tau_{yx}u + \tau_{yy}v \end{bmatrix} \quad (2.4)$$

The shear stress components are expressed as ;

$$\tau_{xx} = (\mu + \mu_t) \frac{M}{Re} \left(\frac{4}{3} \frac{\partial u}{\partial x} - \frac{2}{3} \frac{\partial v}{\partial y} \right)$$

$$\tau_{yy} = (\mu + \mu_t) \frac{M}{Re} \left(\frac{4}{3} \frac{\partial v}{\partial y} - \frac{2}{3} \frac{\partial u}{\partial x} \right)$$

$$\tau_{xy} = (\mu + \mu_t) \frac{M}{Re} \left(\frac{\partial u}{\partial y} + \frac{\partial v}{\partial x} \right)$$

$$\tau_{yx} = \tau_{xy} \quad (2.5)$$

where ρ is the density, p is the static pressure, H is the total enthalpy per unit volume, e_T is the total energy per unit volume and respectively u and v are the two velocity components in the x and y directions. H , p and e_T are defined as follows with respect to internal energy , e , :

$$e_T = e + \frac{x^2 + y^2}{2}$$

$$p = (\gamma - 1)\rho e$$

$$H = \gamma e + \frac{x^2 + y^2}{2} \quad (2.6)$$

2.2 Turbulence Modeling

Turbulence viscosity needs to be assessed by using one of the turbulence models. In this thesis, eddy viscosity is calculated by using Spalart-Allmaras [13] one equation turbulence model and Detached Eddy Simulation based on Spalart-Allmaras one equation turbulence model. In both turbulence models, transition effect was not taken into account since computations in this study are assumed to be fully turbulent.

2.2.1 Spalart-Allmaras Turbulence Model

Spalart-Allmaras turbulence model is one of the eddy viscosity models and it can be used with the grids of any structure both in 2D and 3D Navier-Stokes solvers. In this model, the transport equation is generated with respect to empiricism and arguments of dimensional analysis, galilean invariance and selective dependence on the molecular viscosity [14]. In order to solve turbulent flows, a single partial differential equation is solved for a variable $\tilde{\nu}$ which is related to the eddy viscosity. In literature, there are various modifications of the Spalart-Allmaras turbulence model. More information about these modifications can be found in Reference [15]. The differential equation which is implemented in its conservative non-dimensional form can be seen in Equation (2.7).

$$\frac{\partial \tilde{\nu}}{\partial t} + u \frac{\partial \tilde{\nu}}{\partial x} + v \frac{\partial \tilde{\nu}}{\partial y} = c_{b1} \tilde{S} \tilde{\nu} - \frac{M}{Re} c_{w1} f_w \left(\frac{\tilde{\nu}}{d}\right)^2 + \frac{M}{Re} \frac{1}{\sigma} [\nabla \cdot ((\nu_L + \tilde{\nu}) \nabla \tilde{\nu}) + c_{b2} (\nabla \tilde{\nu})^2] \quad (2.7)$$

In above equation, the left hand side represents advection term while right hand side represents production, destruction and diffusion terms respectively.

2.2.1.1 Modeling of the Dynamic Eddy Viscosity

The dynamic eddy viscosity ν_t is obtained from

$$\nu_t = \tilde{\nu} f_{\nu_1} \quad (2.8)$$

where the viscous damping function f_{v_1} is given by

$$f_{v_1} = \frac{\chi^3}{\chi^3 + C_{v_1}^3}, \quad \chi = \frac{\tilde{\nu}}{\nu} \quad (2.9)$$

2.2.1.2 Modeling of the Turbulent Production

The production term, $P_\nu = c_{b_1} \tilde{S} \tilde{\nu}$ is modeled with

$$\tilde{S} = f_{v_3} S + \frac{M}{Re} \frac{\tilde{\nu}}{\kappa^2 d^2} f_{v_2} \quad \text{where} \quad (2.10)$$

$$f_{v_2} = \left(1 + \frac{\chi}{c_{v_2}}\right)^{-3} \quad (2.11)$$

$$f_{v_3} = \frac{(1 + \chi f_{v_1})(1 - f_{v_2})}{\max(\chi, 0.001)} \quad (2.12)$$

$$S = |\Omega_{ij}| + C_{prod} \min(0, |S_{ij}| - |\Omega_{ij}|) \quad (2.13)$$

$$|\Omega_{ij}| = \sqrt{2\Omega_{ij}\Omega_{ij}} \quad (2.14)$$

$$|S_{ij}| = \sqrt{2S_{ij}S_{ij}} \quad (2.15)$$

$$\Omega_{ij} = \frac{1}{2} \left(\frac{\partial u}{\partial y} - \frac{\partial v}{\partial x} \right) \quad (2.16)$$

$$S_{ij} = \frac{1}{2} \left(\frac{\partial u}{\partial y} + \frac{\partial v}{\partial x} \right) \quad (2.17)$$

In the above equations, $|\Omega_{ij}|$ is magnitude of vorticity, $|S_{ij}|$ is magnitude of strain, Ω_{ij} is mean rate of rotation tensor and S_{ij} is mean strain rate tensor. In order to avoid possible numerical

problems, \tilde{S} should not be zero or negative. Also, d represents closest distance to the nearest wall.

2.2.1.3 Modeling of the Turbulent Destruction

The destruction term reduces the eddy viscosity in the log layer and laminar sublayer. The destruction term $Y_v = \frac{M}{Re} c_{w1} f_w (\frac{\tilde{v}}{d})^2$ is modeled with

$$f_w = g \left[\frac{1 + c_{w3}^6}{g^6 + c_{w3}^6} \right]^{\frac{1}{6}} \quad (2.18)$$

$$g = r + c_{w2} (r^6 - r) \quad (2.19)$$

$$r = \min \left[\frac{M}{Re} \frac{\tilde{v}}{\tilde{S} \kappa^2 d^2}, 10 \right] \quad (2.20)$$

The constants are :

$$c_{b1} = 0.1355 \quad c_{b2} = 0.622 \quad \sigma = \frac{2}{3} \quad \kappa = 0.41 \quad c_{v1} = 7.1$$

$$c_{w1} = \frac{c_{b1}}{\kappa^2} + \frac{(1+c_{b2})}{\sigma} \quad c_{w2} = 0.3 \quad c_{w3} = 2.0 \quad C_{prod} = 2.0$$

$$c_{v2} = 5.$$

In order to adopt differential form of Spalart-Allmaras turbulence model into the integral form, divergence theorem is applied to convective and diffusive fluxes and Equation (2.7) is integrated over a control volume. In addition, overflow/underflow may occur if the production and destruction terms are not implemented properly.

$$\begin{aligned} \frac{\partial}{\partial t} \int_{\Omega} \tilde{v} d\Omega + \oint_S \tilde{v} \mathbf{U} \cdot \mathbf{n} dS - \oint_S \frac{M}{Re\sigma} (v + \tilde{v}) \nabla \tilde{v} \cdot \mathbf{n} dS \\ = \int_{\Omega} [P_v - Y_v + \frac{M}{Re\sigma} c_{b2} (\nabla \tilde{v})^2] d\Omega \end{aligned} \quad (2.21)$$

The boundary conditions are :

$$\tilde{v}_{wall} = 0$$

$$\tilde{v}_{farfield} = 3v_{\infty}, \therefore, 5v_{\infty}$$

2.2.2 Detached Eddy Simulation Method

Detached Eddy Simulation (DES) is introduced firstly in 1997 by Spalart for seperated flows in high Reynolds numbers. In this method, while entire boundary layer is predicted with one of the RANS closure model, the seperated regions are calculated by LES. DES turbulence model give the same results with RANS in the attached flows at low angle of attack. Travin et al defined the first version of DES ,known as DES97, as “*a three-dimensional unsteady numerical solution using a single turbulence model, which functions as a subgrid-scale model in regions where the grid density is fine enough for a large-eddy simulation, and as a Reynolds-averaged model in regions where it is not.*”[16] In this thesis, DES model based on Spalart-Allmaras one equation turbulence model,DES97, is used.

2.2.2.1 Spalart-Allmaras Based DES Model

In Spalart-Allmaras based DES model, distance to the closest wall ,d, is replaced everywhere with a new length scale \tilde{d} in the Spalart-Allmaras model.

$$\tilde{d} = \min(d, C_{DES} \Delta) \quad (2.22)$$

where C_{DES} ,being the DES coefficient, is equal to 0.65 for homogeneous turbulence. Δ is the filter width and plays important role in turbulence modeling especially in hybrid turbulence models due to the fact that switching from RANS to LES depends on it. Δ represent the greatest local grid distance and there are various choice of an expression for the filter width. Some of them can be seen below. In this study, expression of local grid distance is taken like presented in Equation (2.23).

$$\Delta = \max(\Delta_x, \Delta_y) \quad (2.23)$$

$$\Delta = (\Delta_x \Delta_y)^{\frac{1}{2}} \quad (2.24)$$

$$\Delta = \left(\frac{\Delta_x^2 + \Delta_y^2}{2} \right)^{\frac{1}{2}} \quad (2.25)$$

Close to the wall ,where $d < \tilde{d}$, the model employs as Spalart-Allmaras turbulence model and away from the wall ,where $d > \tilde{d}$, the model turns into LES with smagorinsky SGS model. In case d and \tilde{d} at the same order, the space between RANS and LES area problematic and still it is not known exactly what actually happens. This is known as grey area problem.

2.2.3 Grid Generation

In order to obtain numerical solution, the domain of the selected test case must be meshed by mesh generators. Generally, hybrid C-type and hybrid O-type grids are used in simulating flow over airfoils. Although generation of O-type hybrid grid requires just one face by Gambit 2.4.6 for the solution of flow around airfoils , boundary layer cell transition in sharp edges are very bad. It is clearly seen in Figure 2.1 that the last boundary layer cell on the trailing edges is 100 times bigger than its neighbouring cell near wall. As presented in Figure 2.2 in hybrid C-type type grids boundary layer cell transition in sharp edges are smooth. Therefore, in this study Hybrid C-type grids are used in all simulations.

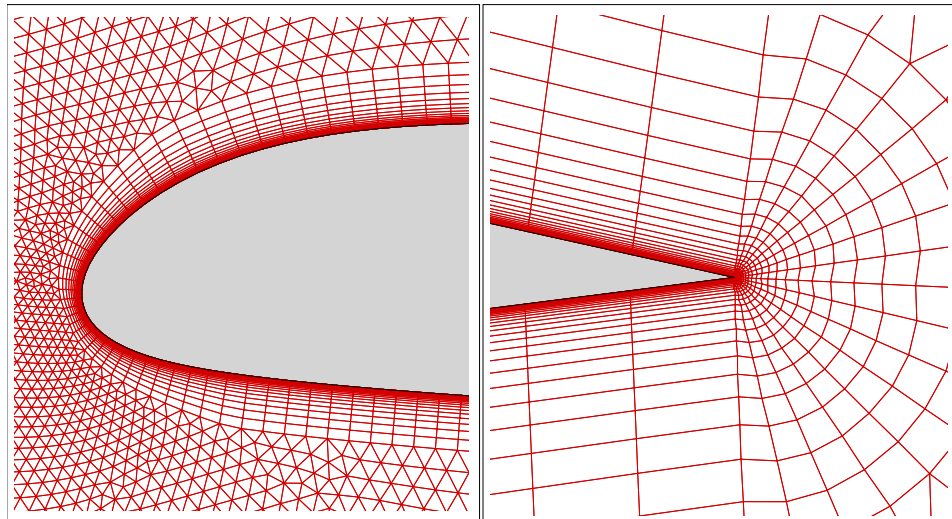


Figure 2.1: Zoomed View of Hybrid-O Grid for Aerospace Airfoil

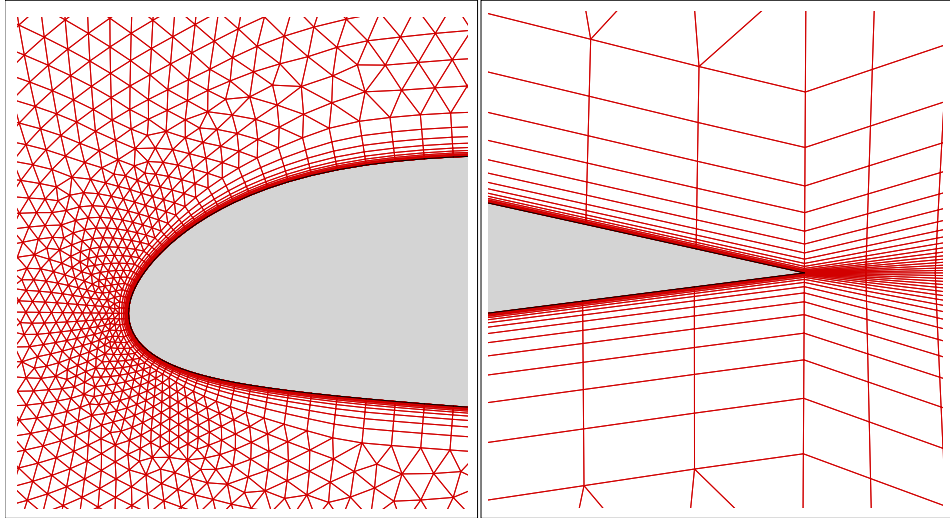


Figure 2.2: Zoomed View of Hybrid-C Grid for Aerospatiale Airfoil

Generated hybrid grids contain triangular-quadrilaterals cells and quadrilaterals cells are just clustered near walls. In DES turbulence model, grid generation is one of the most important issue and it has a special grid type which is called DES grid. Spalart [18] clarified the critical points about DES grid. In basic, DES grid has two regions. RANS region is affective near walls and requires both fine mesh for the boundary layer treatment and high aspect ratio cells for reducing cell numbers. While Spalart-Allmaras model requires y^+ value between $5 < y^+ < 30$ for obtaining good result without wall functions, DES requires y^+ around $y^+ \approx 1$. Additionally, the stretch ratio should not exceed 1.15 value. In order to estimate first layer thickness in the geometries which are not actually a flat plate, the expression given in [45] is used. In this expression, first layer thickness is a function of the Reynolds numbers and can be seen in Equation (2.26).

$$y^+ = 0.172yRe^{0.9} \quad (2.26)$$

where y is the non-dimensional first layer thickness and Re is the flow Reynolds numbers based on the chord length. LES region is the rest of the domain and the mesh should be isotropic. Although this cause a respectable increase in cell size, the smaller the size of cells, the more the cells are simulated.

Because Gambit exports the mesh in neutral file format, a small Fortran code is used for the purpose of converting neutral mesh file (mesh.neu) to solver's input mesh file (mesh.dat). SET2D is used cell based data structure. Cell based data structure lists the connectivity of

each cell with its nodes and neighbouring cells numbers. Note that there are ghost cells on the far field and airfoil surface. The cell number values of ghost cells are taken -1 in farfield and -2 in walls as a boundary condition value. In Figure 2.3, how node and cell numbers are located on the solution domain is presented and an example of grid file can be seen in Appendix C.

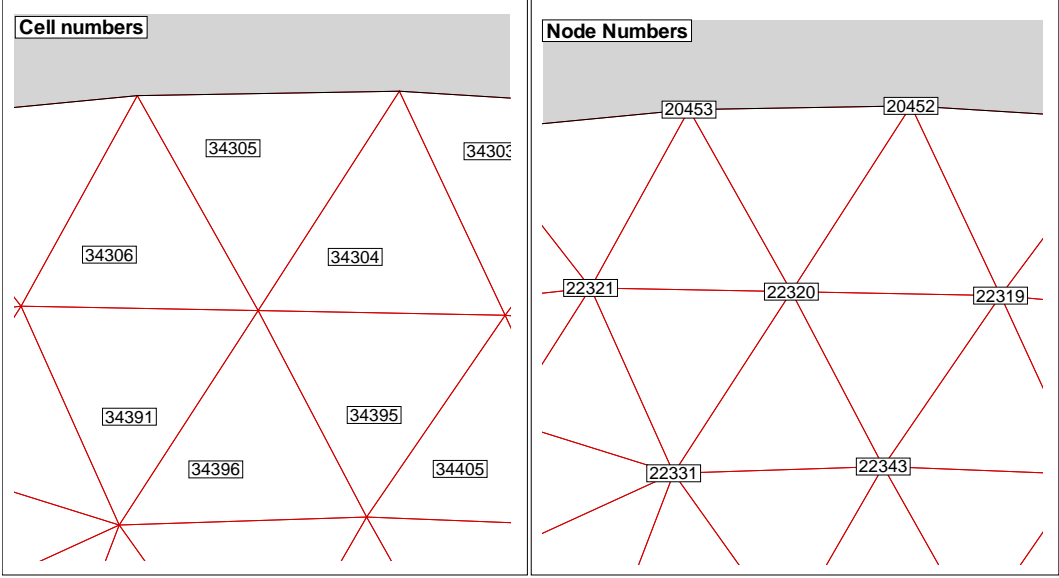


Figure 2.3: Node and Cell Numbers of Triangular Cells

2.3 Numerical Method

In CFD to obtain solution after generating the grid and defining the geometrical quantities the next step is to discretize the governing equations.

2.3.1 Spatial Discretization

Spatial discretization is a numerical method to calculate the convective and diffusive fluxes. In this study, convective and diffusive fluxes are approximated by cell centered finite volume method. Equation 2.1 becomes after discretization for each cell as below.

$$\Omega \frac{\partial}{\partial t} Q + \sum_1^{n \text{ face}} (F \Delta y - G \Delta x) = \sum_1^{n \text{ face}} (F_v \Delta y - G_v \Delta x) \tag{2.27}$$

In the Equation (2.27), Ω is the area of the cell and Δx , Δy are face lengths of the cell. While the inviscid fluxes, F and G , are calculated at the faces of the cells by using upwind methods, the viscous fluxes are calculated at the faces of the cells after computing the gradients of the conservative quantities.

2.3.1.1 Calculation of the Gradients

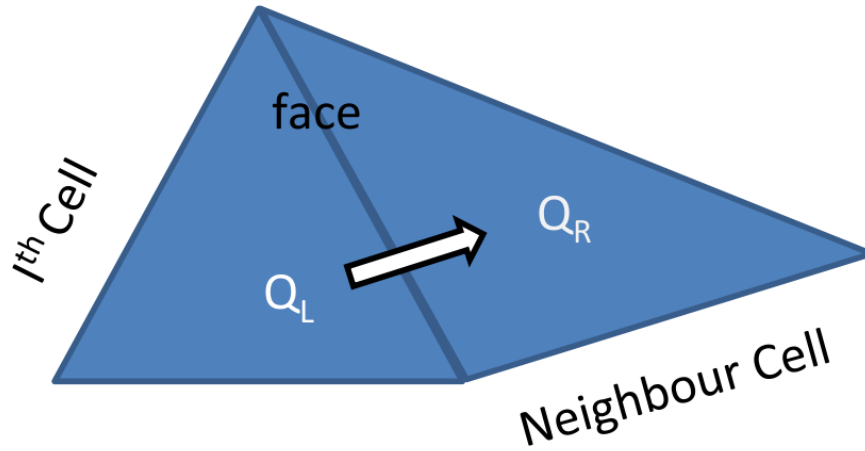


Figure 2.4: A Cell with Its Neighbours

First of all, fluxes at each edges in the cells are calculated from;

$$q_{face} = \frac{q_R + q_L}{2}$$

Then, the gradients of any quantity can be calculated using Green's Gradient Theorem which is given as follows;

$$\nabla \Phi = \frac{1}{\Omega} \oint_S \Phi \mathbf{ds} = \frac{1}{\Omega} \sum_{m=1}^{n \text{ face}} \Phi (\Delta y_m \mathbf{i} - \Delta x_m \mathbf{j})$$

After the calculation of the gradients at each cell, the face average gradients are used to calculate the viscous stresses at the face centers.

2.3.2 Temporal Discretization

In this study, time marching is obtained by employing the explicit three-stage Runge-Kutta time stepping method for the flow variables and one stage Euler scheme for the Spalart-Allmaras based DES turbulence model.

$$\frac{\partial}{\partial t} Q = -\frac{1}{\Omega} \sum_1^{n \text{ face}} [(F - F_v) \Delta y - (G - G_v) \Delta x] = -\frac{1}{\Omega} R \quad (2.28)$$

In the Equation (2.28), R represents the total numerical flux at the cell, called as the Residual and discretised as ;

$$\Delta Q^n = -\frac{\Delta t}{\Omega} R^n \quad \text{where} \quad \Delta Q^n = Q^{n+1} - Q^n \quad (2.29)$$

Equation (2.30) can be rearranged to obtain Q^{n+1} as;

$$Q^{n+1} = Q^n - \frac{\Delta t}{\Omega} R^n \quad (2.30)$$

2.3.2.1 Runge-Kutta Three Stage Method

The three stage Runge-Kutta method is employed as Jameson et al.[44] described. The flow quantities at $(n + 1)^{th}$ time step are obtained from the quantities $(n + 1)^{th}$ time step in three stages.

$$\begin{aligned} Q^0 &= Q^n \\ Q^1 &= Q^0 - \alpha_1 \frac{\Delta t}{\Omega} R^0(Q^0) \\ Q^2 &= Q^0 - \alpha_2 \frac{\Delta t}{\Omega} R^1(Q^1) \\ Q^3 &= Q^0 - \alpha_3 \frac{\Delta t}{\Omega} R^2(Q^2) \\ Q^{n+1} &= Q^3 \end{aligned} \quad (2.31)$$

where Δt is the time step and the stage coefficients used are ;

$$\alpha_1 = \frac{1}{3}, \quad \alpha_2 = \frac{1}{2}, \quad \alpha_3 = 1$$

This scheme is used for both steady and unsteady flow predictions. In unsteady flow calculations, time step is set to global constant value which is the time step of the smallest cell. On the other, hand for the steady state calculations, local time step is used for each cell.

Time step is limited by the stability criteria set by the CFL condition. In explicit time integration, CFL coefficient must be between one and zero. As CFL number gets bigger, the information goes further in the solution domain and the convergence time decreases. Local time stepping is used to accelarete the convergence of the solution toward the steady state.

2.3.3 Parallelization of the Code

Turbulent flow simulations require too much time consuming calculations therefore, parallel environment becomes indispensible tool in these simulations. The parallel version of SET2D is based on the domain decomposition of the grid. Partial Virtual Machine (PVM) libraries are used to pass information between the processors. METIS is used to partition the grid into zones. Figure 2.6 shows the flow chart for the parallel Set2d Navier-Stokes solver.

2.3.3.1 Partial Virtual Machine

PVM is a software developed by the Heterogeneous Network Project initiated in 1989 to generate a set of heterogeneous computers connected by a network to appear as a one large computer resource. Operating system which is running on hosts can be homogenous or heterogeneous. C, C++ and Fortran programming languages are supported. PVM is based on master-worker paradigm. In PVM, one should write one master and one worker code to paralellize the serial code. While master code initializes the solution, organizes the task of worker and combine final results of workers, worker code ensures the communication between workers and sends final results to master.

2.3.3.2 Domain Decomposition

Domain decomposition is defined as partitioning the solution domain into sub-domains of equal size to achieve load balancing since the load balancing and communication overhead items are the most crucial points in parallel performance. The hybrid grids are partitioned by using METIS software package. An example of domain decomposition performed by METIS for Aerospatiale airfoil can be seen in Figure 2.5. Each color represents a different partition.

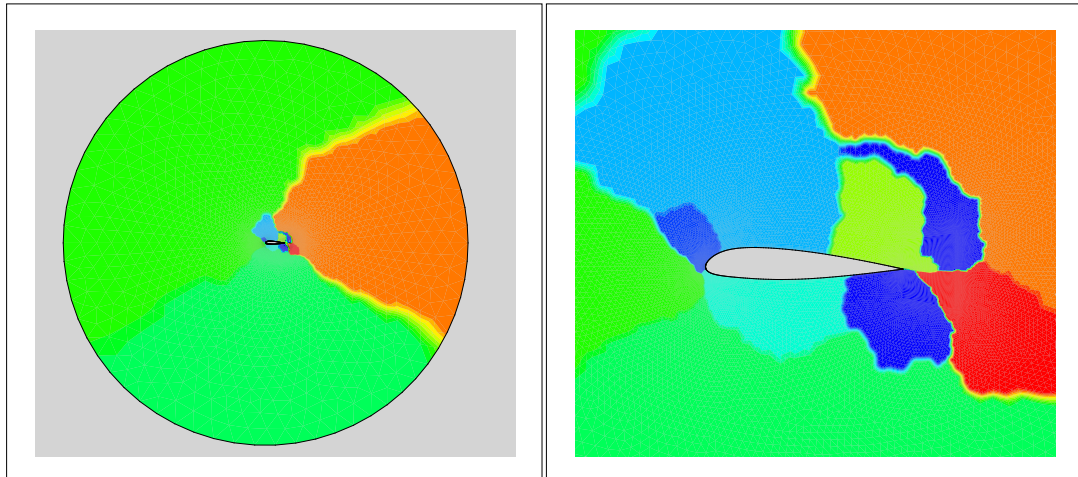


Figure 2.5: Sample Domain Decomposition for Aerospatiale Airfoil by Using METIS Software Package (10 partitions)

2.3.3.3 Parallel Computing Environment

The parallel computing environment comprise of networked PCs running a Linux operating system. There are 6 computers (atmaca 4x/5x series) with dual Xeon processors. The data between processors is transferred by a 1 Gbps ethernet switch.

2.3.3.4 Boundary Conditions

Boundary conditions are very important initial concept and requires a particular attention since improper set of boundary conditions can cause nonphysical effects on the solution. In parallel environment, the solution in one part depends on neighbouring partitions. Therefore, conservative and turbulence variables must be sent correctly to neighbouring cells at each iteration by means of interfacing boundary conditions.

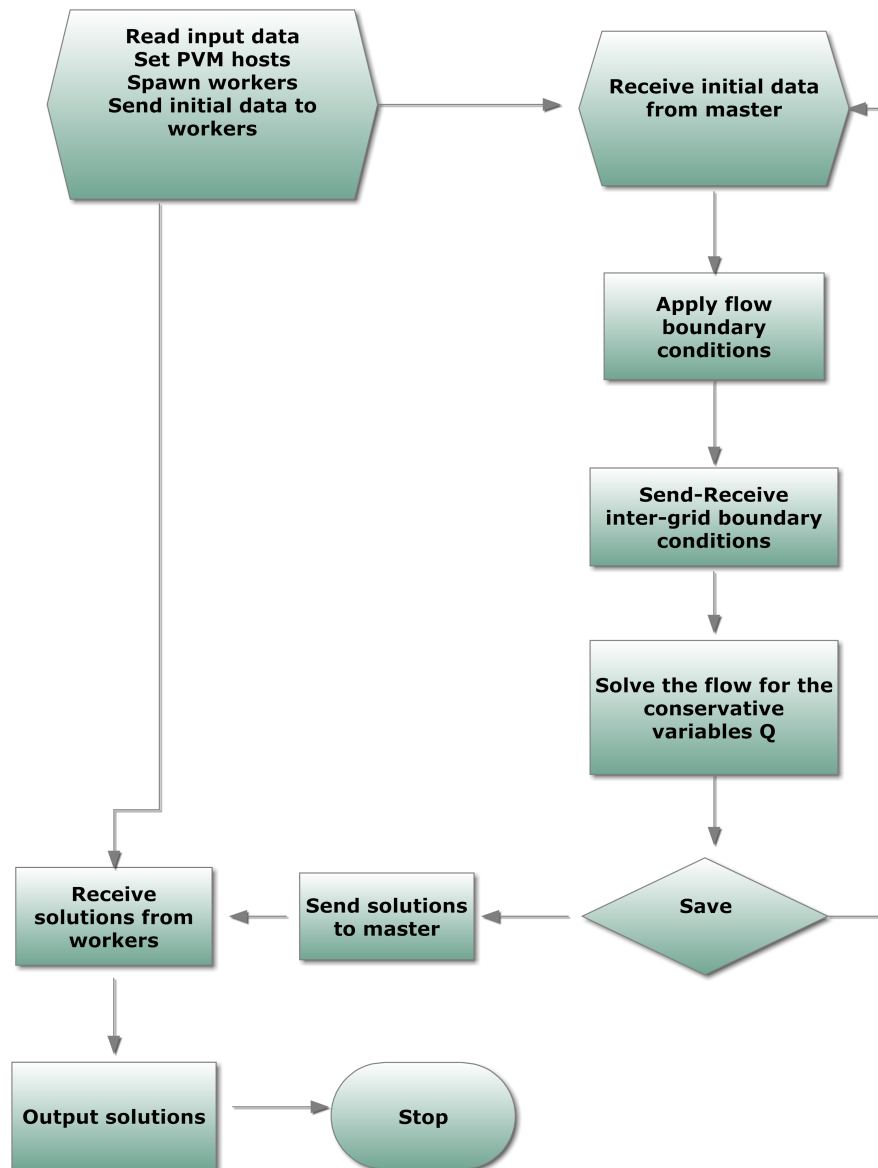


Figure 2.6: Flow Chart of the Parallel Code

CHAPTER 3

RESULTS AND DISCUSSION

In this chapter, first of all parallel validation of implemented DES turbulence model is done at transonic flow solutions over RAE2822 airfoil for steady state flow condition. Then, parallel performance of the Set2d solver is tested. Lastly, performance of Spalart-Allmaras and DES turbulence models of Set2d solver are analyzed at flow over Aerospatiale and NACA 0015 airfoils. Obtained results are compared against available datas and results of Fluent solver. Results of each test case are presented in corresponding sections.

3.1 Validation Case : Transonic Flow Solutions over RAE2822 Airfoil for Steady-State Flow Condition

In this validation case, two dimensional, transonic, turbulent flow over RAE2822 airfoil referred as AGARD case9 is studied with Hybrid-grids. For steady-state flow condition, the effect of grid density resolution, y^+ value and C_{DES} coefficient on solutions are investigated with DES97 turbulence model. Also, the performance of parallel computing is investigated. The obtained pressure and skin friction distributions are compared both with the experimental data which is found in AGARD Advisory Report no. 138 [46] and numerical solution of Chit et al. [47]. Chit et al. developed a gas kinetic solver with combined $k - \epsilon/k - \omega$ SST two equation turbulence model. While inviscid fluxes are calculated by second order spatial accuracy Monotone Upstream Centered Schemes, time integration is achieved by fourth order Runge-Kutta method for steady state flow.

The solution is assumed to reach steady state when the reduction of density residual is less than four order of magnitude in turbulent flow cases. The free stream conditions can be seen in Table 3.1.

Table 3.1: Free Stream Flow Conditions for RAE2822

Mach Number	Reynolds Number	α	CFL Number	Reference
0.73	$6.5E + 6$	2.8°	0.95	[46],[47]

3.1.1 Effect of Grid Density on the Solution

The effect of grid density on solution is investigated with C-type hybrid grids which have different grid resolution. Table 3.2 summarizes the features of the used grids. Figure 3.1

Table 3.2: Characteristics of Used Grids for Turbulent Flow over RAE2822 Airfoil

Mesh	# of nodes over airfoil surfaces	# of nodes	# of cells	y^+
Mesh-160	160	9362	14996	$y^+ \approx 0.95$
Mesh-320	320	16627	26026	$y^+ \approx 0.95$
Mesh-440	440	24026	38058	$y^+ \approx 0.95$
Mesh-600	600	34141	54122	$y^+ \approx 0.95$

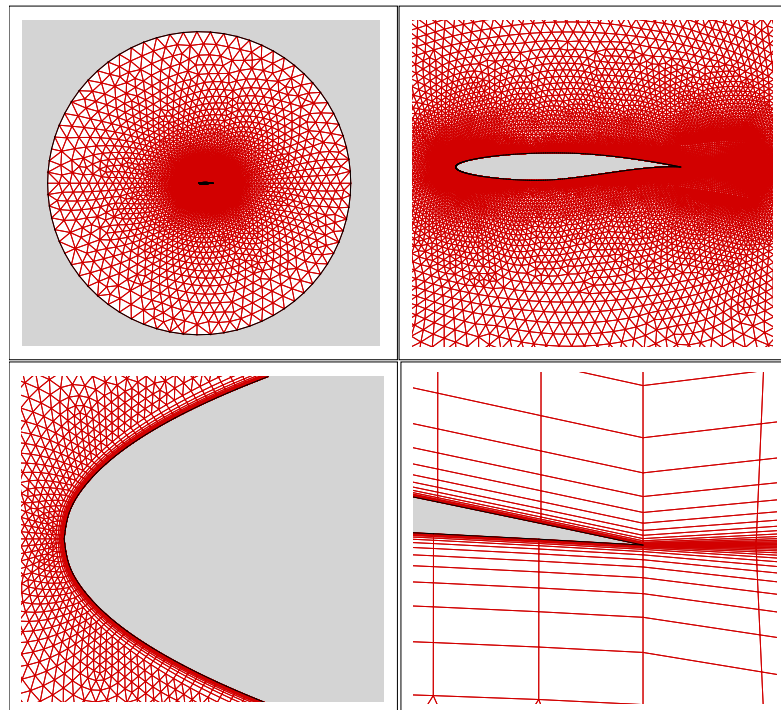


Figure 3.1: Detailed view of Mesh-440

shows close up views of Mesh-440 solution domain. All of the grids have the same topology. The chord length of RAE2822 airfoil is 1 unit while farfield boundary is taken as 11 units. The distance from the first layer of the boundary layer to the closest wall is 2×10^{-6} units.

Figure 3.2 presents residual histories for different grids. After 50000 iterations, at least four order drop in density residual and five order drop in turbulent viscosity are obtained. This is sufficient to accept that the solution is converged for all mesh resolutions.

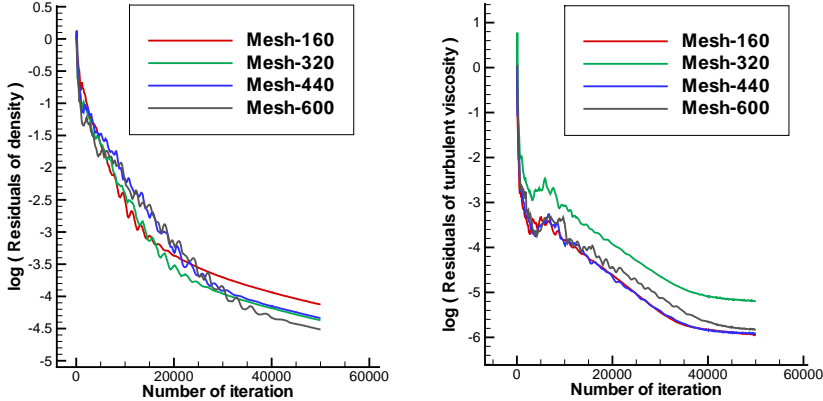


Figure 3.2: Converge History of Different Grids

The pressure and skin friction coefficient distributions along the chord length are given in Figure 3.3. It is clearly seen from Figure 3.3 that the computed results of all grids except

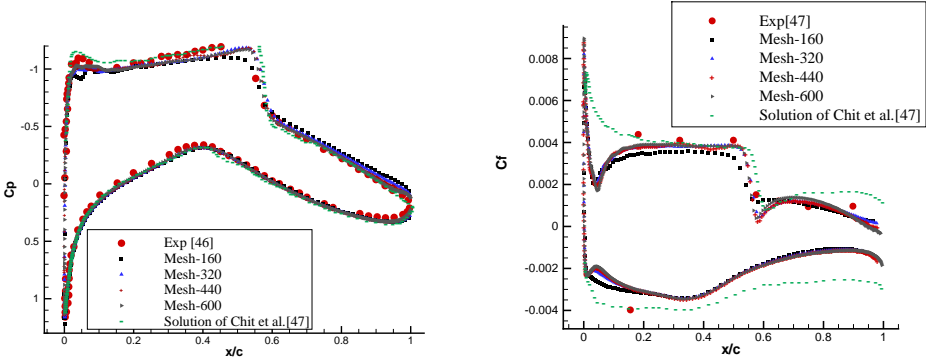


Figure 3.3: Pressure and Skin Friction Coefficient Distrubition

Mesh-160 give similar solutions. This is a desired feature of solver, since grid independence is achieved. C_p distribution results agree well with AGARD experimental data. Skin friction

distribution over airfoil is reasonable when compared with experimental data and computational result of Chit et al. [47]. Both in upper and lower side of the airfoil, peak skin friction of the leading edge is underpredicted. This attributed to the fully turbulent flow assumption and first order accurate solutions. The computational performance of the Set2d-DES turbulence model for this case is compared with the aid of Table 3.3. In order to reduce communication time, only one host with eight cpu is used in all computations. Mesh-440 and Mesh 600 named solution domains give the same pressure and skin friction distribution over airfoil. Since Mesh-440 needs less time and memory than Mesh-600, Mesh-440 named solution domain will be used for other sub-studies.

Table 3.3: Computational Details of Used Grids for Turbulent Flow over RAE2822 Airfoil

Mesh	# of processors	Cpu time (Minute)	Memory requirement (MB)	# of iteration
Mesh-160	8	23	15	50000
Mesh-320	8	41	26	50000
Mesh-440	8	62	37.8	50000
Mesh-600	8	90	54	50000

3.1.2 y^+ Effect on the Solution

In this sub-section, y^+ effect is investigated for three different y^+ values. Node number over the airfoil surface is kept constant and features of these grids are given in Table 3.4.

Table 3.4: Y^+ Values of Used Grids for Turbulent Flow over RAE2822 Airfoil

Mesh	# of nodes over airfoil surfaces	# of nodes	# of cells	y^+
Mesh- $y^+ = 0.95$	440	24026	38058	$y^+ \approx 0.95$
Mesh- $y^+ = 0.5$	440	24094	38194	$y^+ \approx 0.5$
Mesh- $y^+ = 0.1$	440	26363	40652	$y^+ \approx 0.1$

Residual histories are presented in Figure 3.4. At least, a reduction of four order of magnitude in density and five order of magnitude in turbulent viscosity residuals are achieved.

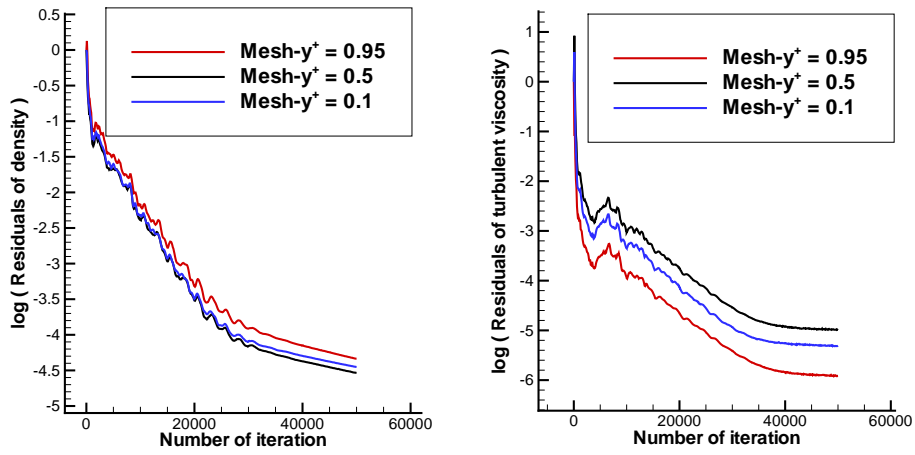


Figure 3.4: Converge History of Mesh-440 Solution Domain for Different y^+ Values

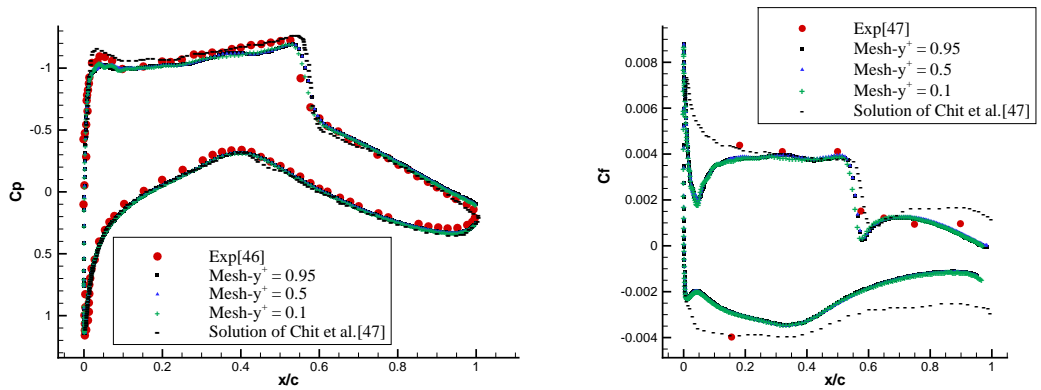


Figure 3.5: Pressure and Skin Friction Coefficient Distribution

The pressure and skin friction distributions over airfoil for different y^+ value are demonstrated in Figure 3.5. It is seen that different y^+ values do not make any change on the solution. This shows that $y^+ \leq 1$ value is enough to obtain turbulent flow solutions.

The computational performance of the Set2d-DES turbulence model for this case is compared with aid of Table 3.5. The elapsed time and required memory are nearly same for different y^+ values.

Table 3.5: Computational Details of Used Grids for Turbulent Flow over RAE2822 Airfoil

Mesh	# of processors	Cpu time (Minute)	Memory requirement (MB)	# of iteration
Mesh- $y^+ = 0.95$	8	62	37.8	50000
Mesh- $y^+ = 0.75$	8	63	37.9	50000
Mesh- $y^+ = 0.5$	8	64	38	50000

3.1.3 Effect of C_{DES} Coefficient on the Solution

In this part, in order to investigate the effect of C_{DES} coefficient on the solution three different C_{DES} values are used. The computations are done for 50000 iterations with Mesh-440. Figure 3.6 presents residual histories for different C_{DES} values. After 50000 iterations, at least four order drop in density residual and six order drop in turbulent viscosity are obtained.

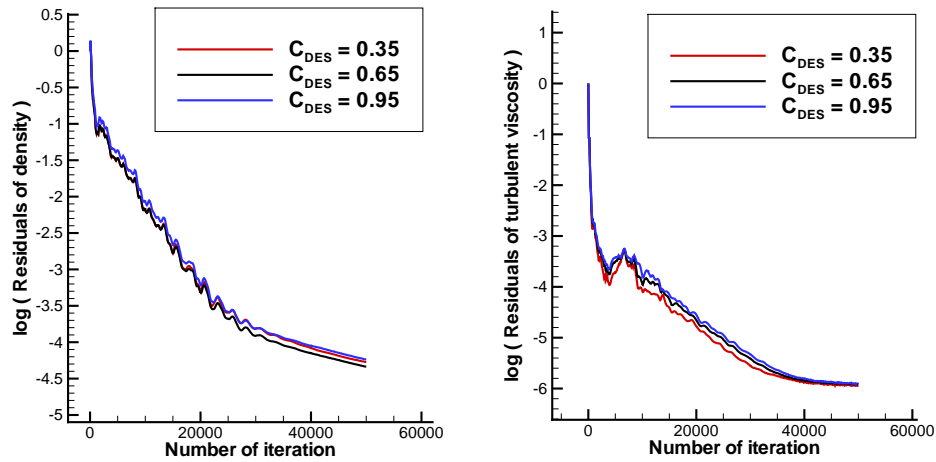


Figure 3.6: Converge history of Mesh-440 solution domain for different C_{DES} coefficient values

The pressure and skin friction coefficient distribution along the chord length is given in Figure 3.7. When C_{DES} is equal to 0.95 and 0.65, the pressure and skin friction distributions agree well with experimental data and the numerical result of Chit et al. If C_{DES} is equal to 0.35, near the trailing edge at the upper side of the airfoil diverge from the correct result is observed. This is attributed to the Modeled Stress Depletion. Modeled Stress Depletion is defined by Spalart et al [23]. Modeled Stress Depletion reduces the skin friction which can lead to

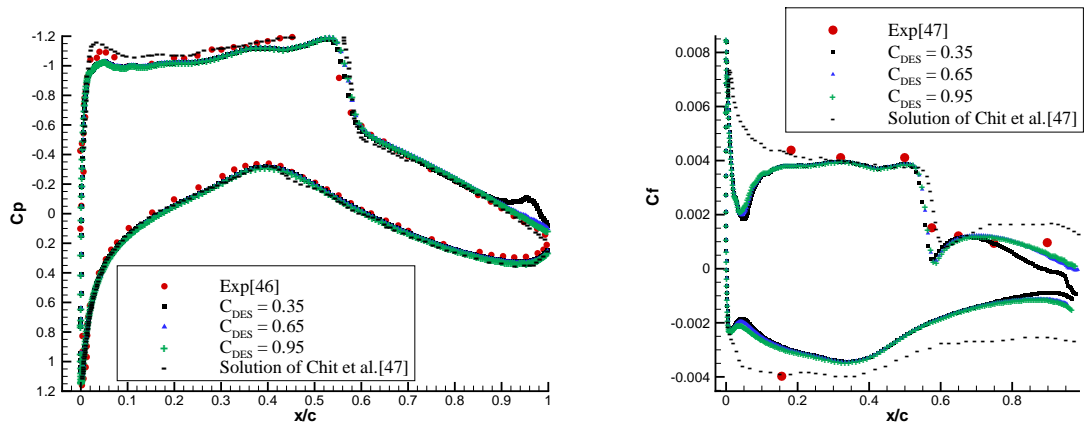


Figure 3.7: Pressure and Skin Friction Coefficient Distribution

premature separation.

The Mach number and turbulent viscosity ratio fields of the turbulent flow over RAE2822 airfoil for different C_{DES} coefficient are compared in Figure 3.8. Although Mach number fields are similar with each other both quantitatively and qualitatively, turbulent viscosity ratio fields are different. As it can be seen from Figure 3.8, C_{DES} coefficient and turbulent viscosity ratio are proportional in DES.

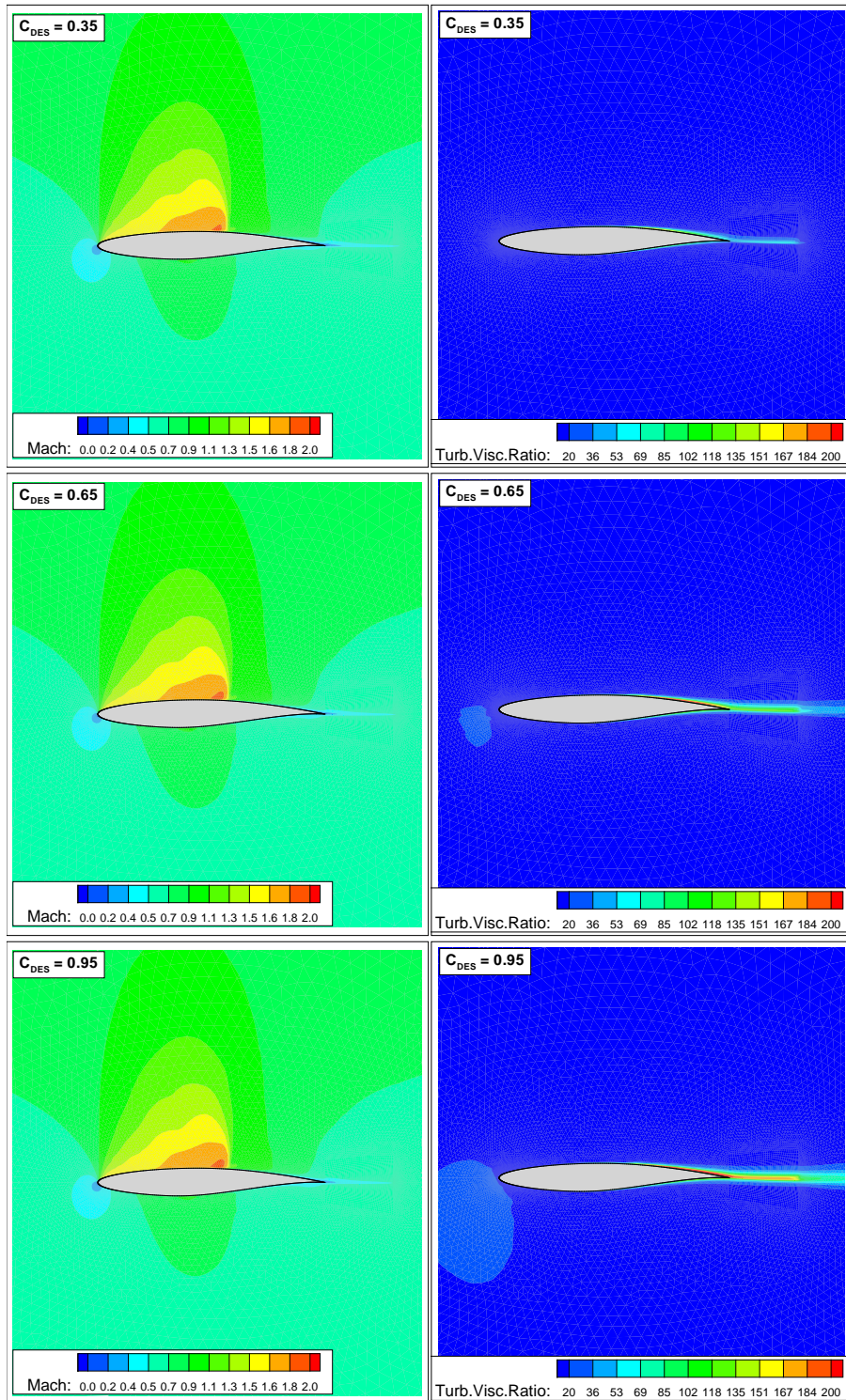


Figure 3.8: Contours of Turbulent Eddy Viscosity of Mesh-440 Solution Domain for Different C_{DES} Coefficient Values

3.2 Performance of Parallel Computing

The parallel performance of Set2d Navier-Stokes code is investigated with the computational grid of Mesh-440 for 30000 iterations. Information about Mesh-440 solution domain can be found in Table 3.2 and detailed view of this solution domain can be seen in Figure 3.1.

Performance of parallel computing is investigated with respect to CPU time. The speed-up of the code is demonstrated in Figure 3.9. As expected speed-up increases linearly with respect to processors numbers however when twelve and sixteen processors are used, it is observed that speed up slope is decreased. Since each host has eight processors, much more time is spent for communication between computer hosts in the network. Therefore eight processors will be used for parallel solutions of Spalart-Allmaras and DES turbulence models in Set2d Navier-Stokes solver to reduce communication time loses.

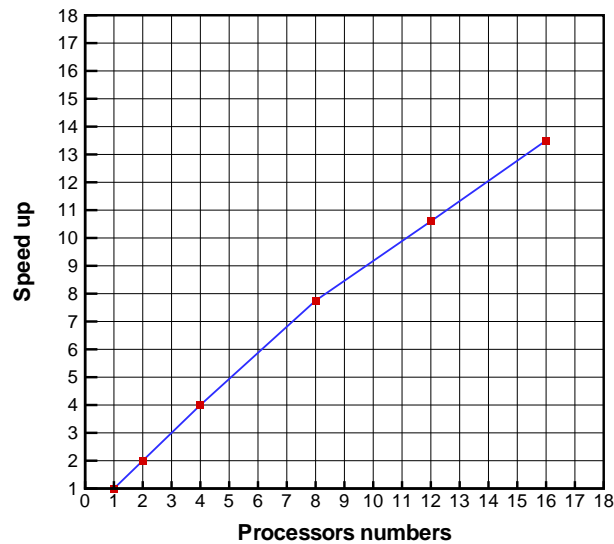


Figure 3.9: Speed up factor for the Mesh-440

3.3 Flow Solutions Over Aerospatale Airfoil

In this case, two dimensional low subsonic flow over Aerospatale ,A-airfoil, airfoil is studied in normal grid resolution. The calculated results are compared with experimental data obtained from [48]. The experiment has been performed in ONERA F2 wind tunnel [49]. In the experiment the Reynolds number and Mach number were 2×10^6 and 0.15 respectively. Measurement under angle of attacks of 7.2° , 12.3° and 13.3° were carried out. Skin friction and pressure distribution over Aerospatale airfoil were measured. Also, mean velocity profiles, Reynolds stresses were measured using a three component LDV system at various chord locations.

For unsteady flow solutions, after the computations start from free stream solution and marches in time with local cell time stepping till density residual drop four order magnitude, global time stepping is used. The free stream flow conditions and some properties of solution domain can be seen in Table 3.6 and Table 3.7 . The chord length of the solution domain is

Table 3.6: Free Stream Flow Conditions for Aerospatale Airfoil

Mach Number	Reynolds Number	α	CFL Number	Reference
0.15	$2.0E + 6$	7.2°	0.95	[48]

Table 3.7: Characteristics of Solution Domain for Turbulent Flow Over Aerospatale Airfoil

Mesh	# of nodes over airfoil surfaces	# of nodes	# of cells	y^+
Mesh-A-airfoil	320	40100	70376	$y^+ \approx 0.95$

taken as 1 unit while the farfield boundary is located 11 chord out from Aerospatale airfoil. The distance from the closest wall to the first boundary layer is 1×10^{-5} units. Detailed view of the solution domain is given in Figure 3.10. Even though y^+ value is adjusted theoretically as $y^+ \approx 0.95$ before simulation by means of Equation (2.26), in fact y^+ value changes over surfaces of the airfoil and also depends on the flow. Actual y^+ distribution over airfoil surface is given in Figure 3.11. This distribution is obtained from Fluent solver. After the solution converged in steady state mode with local time stepping technique, the code is run in unsteady mode with global time stepping technique.

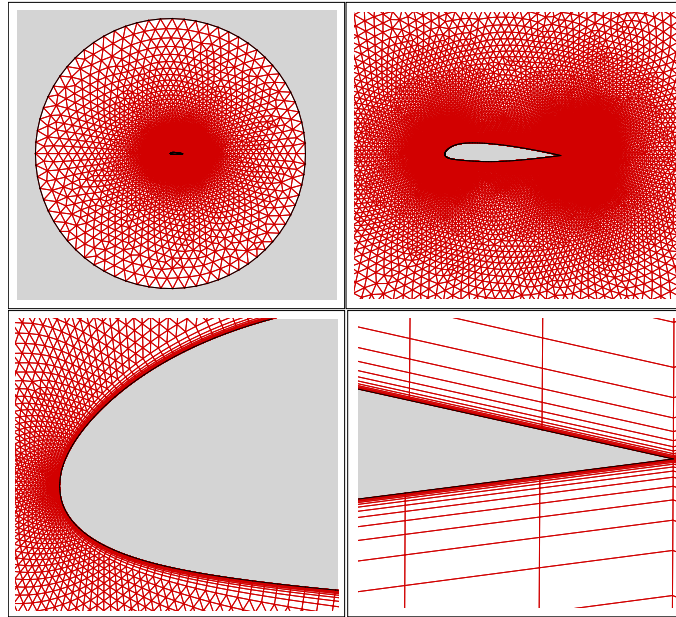


Figure 3.10: Detailed View of Solution Domain for Aerospatiale Airfoil

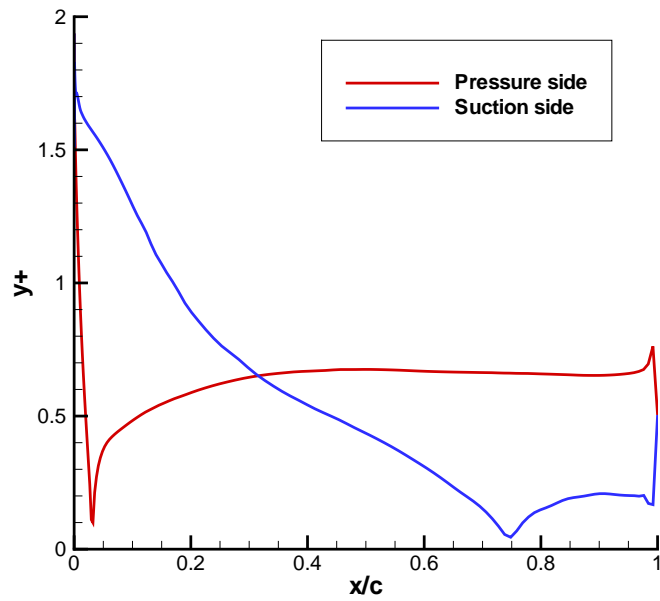


Figure 3.11: Y^+ Distribution over Aerospatiale Airfoil

Computational details of Aerospatiale Airfoil solutions for Spalart-Allmaras and DES turbulence model are presented in Table 3.8. Since DES turbulence model has two length scales

Table 3.8: Computational Details of Spalart-Allmaras and DES Turbulent Model for Turbulent Flow over Aerospatiale Airfoil

Model	# of processors	Cpu time (Minute)	Memory requirement (MB)	# of iteration
SA	8	120	123.2	60000
DES	8	144	123.2	60000

compared to Spalart-Allmaras turbulence model, this costs additional 24 minutes to finish 60000 iterations.

3.3.1 Spalart-Allmaras Turbulence Model Solution

Residual convergence histories can be seen in Figure 3.12. After 60000 iterations, Spalart-Allmaras turbulence model converge to six order magnitude drop in density residual and 5.2 order magnitude drop in turbulent viscosity residual.

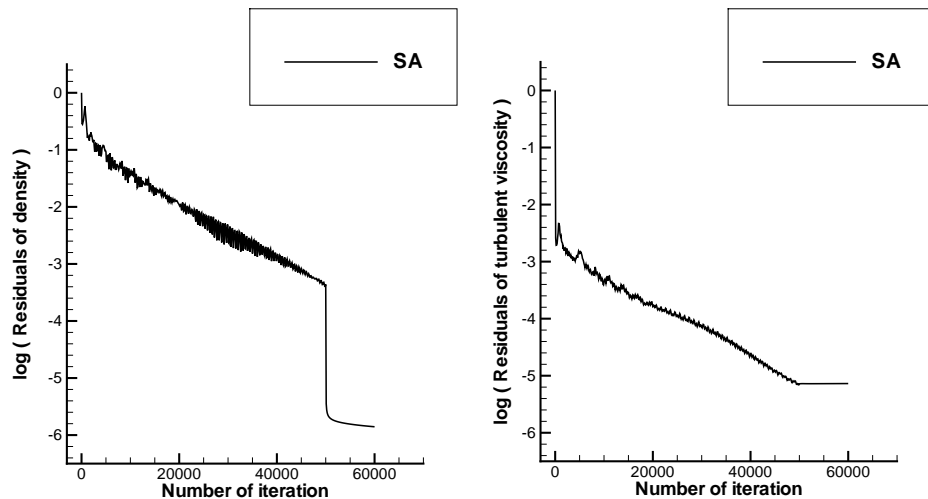


Figure 3.12: Converge History of Residues for Aerospatiale Airfoil

The pressure coefficient distribution over Aerospatiale airfoil is given in Figure 3.13 for Spalart-Allmaras turbulence model. It is clearly seen that, at moderate angle of attack, Set2d-SA gives the same pressure distribution with first order accurate Fluent solver. When compared to experimental data, it is seen that compressible first order solutions of Set2d and Fluent solvers can not catch the suction pressure peak. Since the same solution domain is used both in Fluent and Set2d solvers, the underprediction of the suction peak pressure of the leading

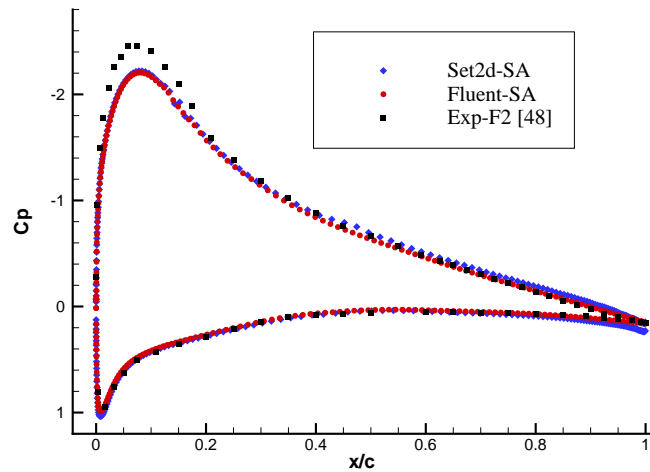


Figure 3.13: Pressure Coefficient Distribution over Aerospace Airfoil for Spalart-Allmaras turbulent model

edge is attributed to the first order accurate solutions. Also fully turbulent assumption may contribute to this. Figure 3.14 compares skin friction distribution on the upper surface of the

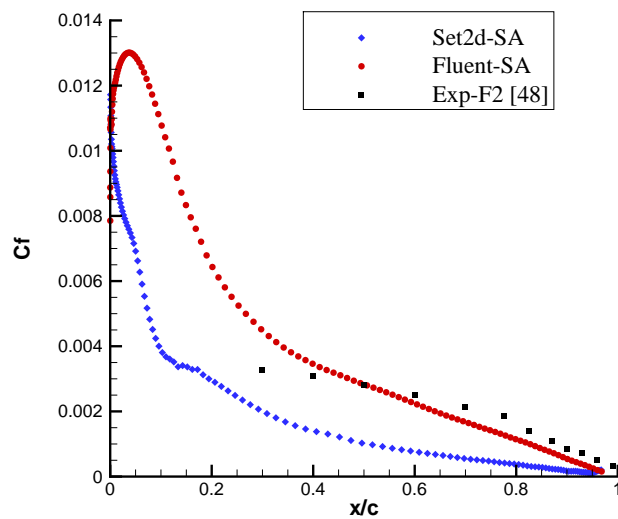


Figure 3.14: Skin Friction Coefficient Distribution over Aerospace Airfoil for Spalart-Allmaras turbulent model

airfoil for Spalart-Allmaras turbulence model. Experimental data comparison with numerical results of both Fluent and Set2d solvers are made. It is seen that while Fluent overpredicts the skin friction coefficient, Set2d underpredicts it. Since first order accurate solutions unsuffi-

cient to calculate velocity gradients correctly, and also experimental results contain 3D effect, 2D simulations fail to calculate skin friction distributions over airfoil correctly. The Mach

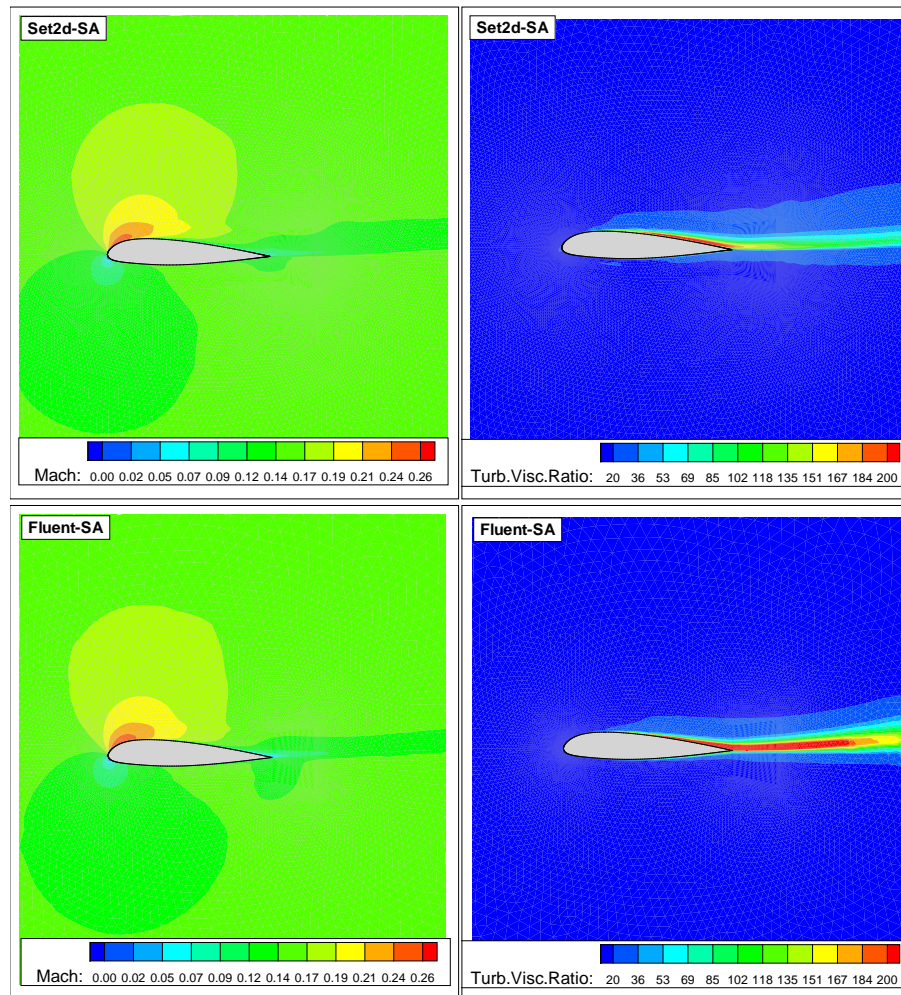


Figure 3.15: Mach Number and Turbulent Viscosity Ratio Contours for Aerospatiale Airfoil

number and turbulent viscosity ratio contours of Aerospatiale airfoil, which are obtained from Fluent and Set2d solvers, are given in Figure 3.15. Obtained results for Mach number fields of Set2d-SA turbulence models are very much alike and agree well with Fluent solver solution. Set2d-SA solution of turbulent viscosity ratio field is less than Fluent-SA turbulent viscosity ratio field. Production of turbulence in Fluent is more than the Set2d solver in the wake of the airfoil. Since the solvers are run at the same state of affairs, this difference is attributed to the wall function. Fluent solver uses wall function but Set2d do not use it.

3.3.2 DES Turbulence Model Solution

Residual convergence histories can be seen in Figure 3.16. After 60000 iterations, DES turbulence model converge to six order magnitude drop in density residual and 4.8 order magnitude drop in turbulent viscosity residual.

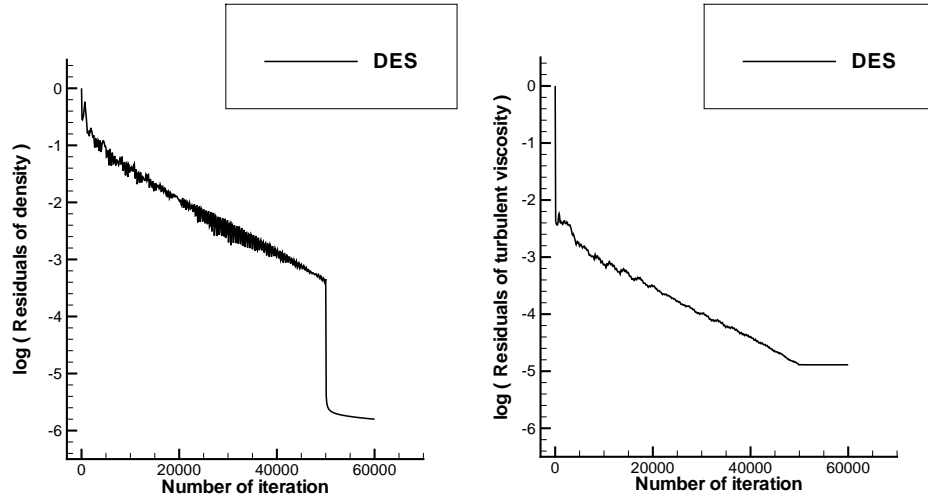


Figure 3.16: Converge History of Residues for Aerospatiale Airfoil

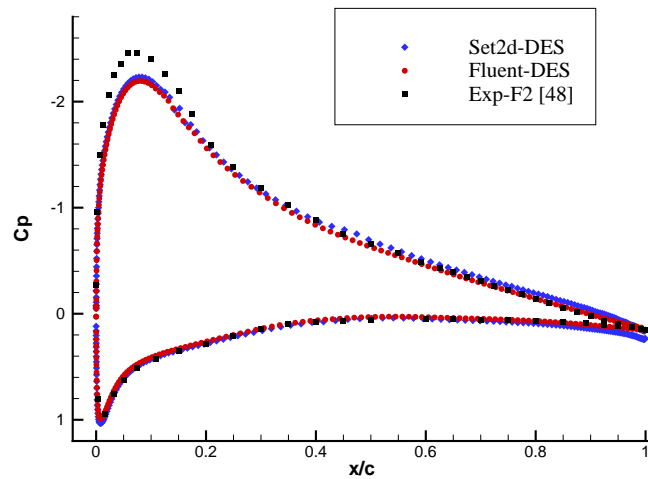


Figure 3.17: Pressure Coefficient Distrubition over Aerospatiale Airfoil for DES turbulent model

The pressure coefficient distribution over Aerospatiale airfoil is given in Figure 3.17 for DES turbulence model. It is clearly seen that, at moderate angle of attack, Set2d-DES gives the

same pressure distribution with Fluent solver. When compared experimental data with Set2d and Fluent solver, it is seen that compressible first order solutions of Set2d and Fluent solvers can not catch the suction pressure peak. Since the same solution domain is used both in Fluent and Set2d solvers, the underprediction of the suction peak pressure of the leading edge is attributed to the first order accurate solutions. Also fully turbulent assumption may contribute to this.

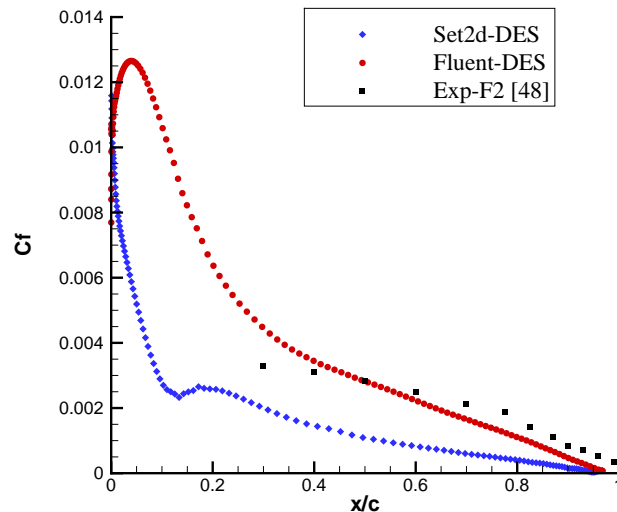


Figure 3.18: Skin Friction Coefficient Distribution over Aerospatiale Airfoil for DES turbulence model

Figure 3.18 compares skin friction distribution on the upper surface of the airfoil for DES turbulence model. Experimental data comparison with numerical results of both Fluent and Set2d solvers are made. It is seen that while Fluent overpredicts the skin friction coefficient, Set2d underpredicts it. Since first order accurate solutions are insufficient to calculate velocity gradients correctly, and also experimental results contain 3D effect, 2D simulations fail to calculate skin friction distributions over airfoil correctly.

The Mach number and turbulent viscosity ratio contours of Aerospatiale airfoil, which are obtained from Fluent and Set2d solvers, can be seen in Figure 3.19. Obtained results for Mach number fields of Set2d-DES turbulence model is very much alike and agree well with Fluent solver solution. Set2d-DES solution of turbulent viscosity ratio fields is less than Fluent-DES turbulent viscosity ratio fields. Production of turbulence in Fluent is much more than the Set2d

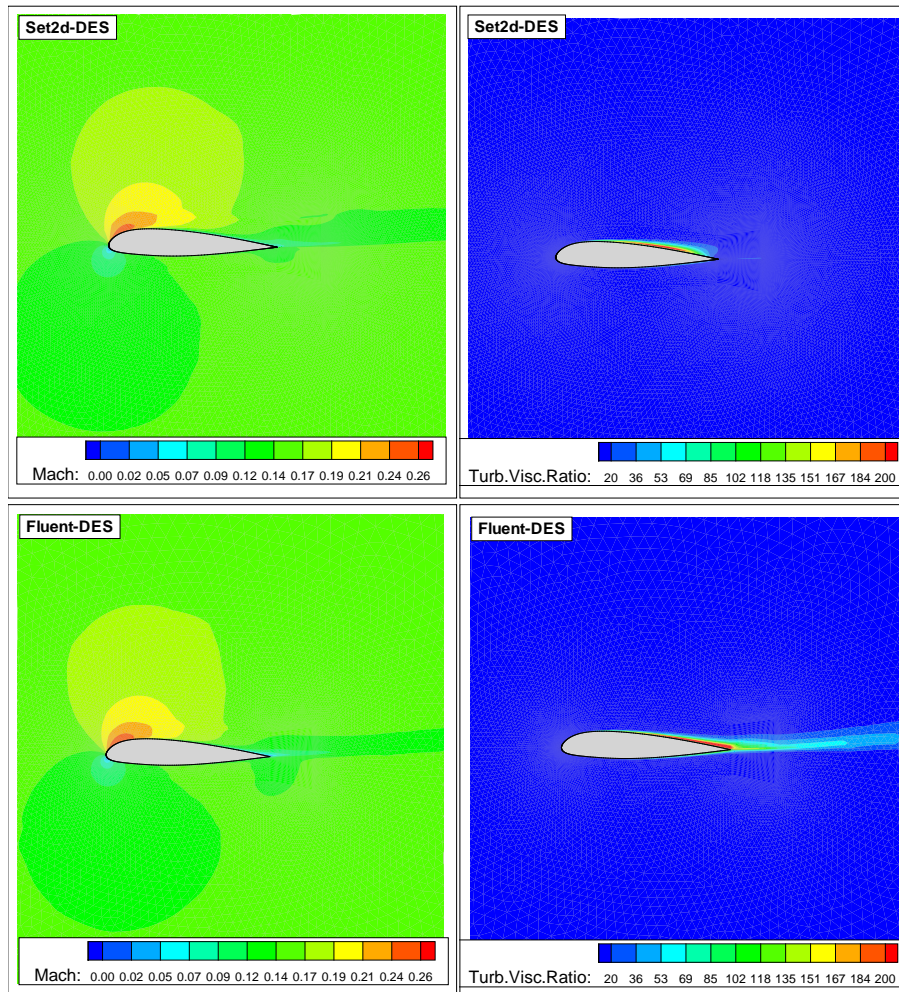


Figure 3.19: Mach Number and Turbulent Viscosity Ratio Contours for Aerospatiale Airfoil solver. This difference is attributed to methodology in calculation of inviscid fluxes. Since Fluent solver constrains to use only Bounded Central-Differencing for calculation of inviscid fluxes in DES turbulence model, its accuracy becomes second order. Therefore Fluent-DES produces more turbulence than Set2d-DES.

3.4 Flow Solutions Over NACA0015 Airfoil at High Angle of Attack

In this section, two dimensional, turbulent, low subsonic flow over NACA0015 airfoil is studied by means of Spalart-Allmaras and DES turbulence models to make comparison with the numerical study of Tu et al. [34]. In their study, they used an incompressible implicit hybrid finite volume/element solver based on DES97. The skin friction coefficient, the pressure coefficient, the aerodynamic coefficients and flow fields are calculated in two dimension with blunt trailing edges for NACA 0015 airfoil.

The free stream flow conditions and some properties of solution domain can be seen in Table 3.9 and Table 3.10 .

Table 3.9: Free Stream Flow Conditions for NACA0015 Airfoil

Mach Number	Reynolds Number	α	CFL Number	Reference
0.1235	$1.5E + 6$	12°	0.95	[34]

Table 3.10: Characteristics of Used Grids for Turbulent Flow Over NACA0015 Airfoil

Mesh	# of nodes over airfoil surfaces	# of nodes	# of cells	y^+
Mesh-NACA0015	440	24317	38460	$y^+ \approx 0.65$

The chord length of the NACA0015 airfoil taken as 1 unit while farfield boundary is taken as 11 units. In the boundary layer, the thickness of the first layer is 1×10^{-5} units. As can be seen in Figure 3.20, sharp trailing edge is used in solution domain. Although, according to Equation (2.26), y^+ value is estimated theoretically, actual y^+ value change over the surfaces and its distribution over the airfoil can be seen in Figure 3.21. This distribution is obtained from Fluent solver after simulation finished. After the solution is converged in steady state mode with local time stepping technique, the code is run in unsteady mode with global time stepping technique.

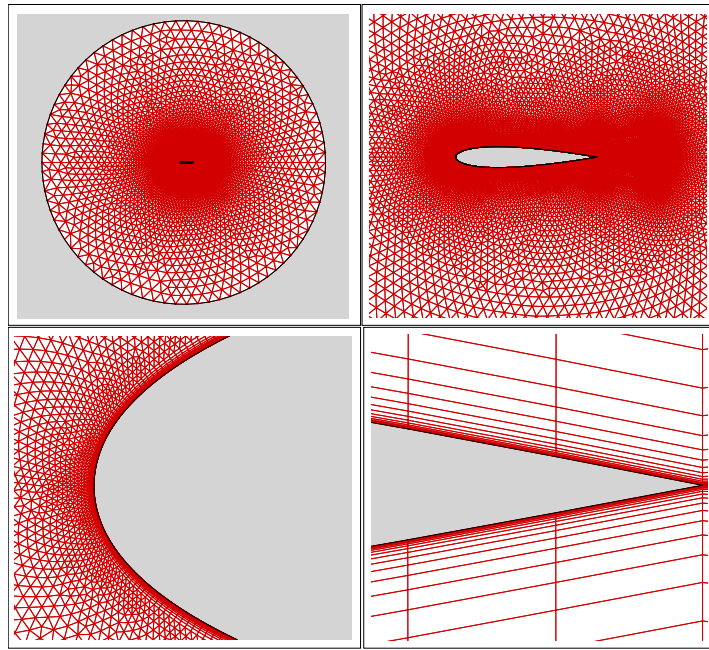


Figure 3.20: Detailed View of Solution Domain for Naca0015 Airfoil

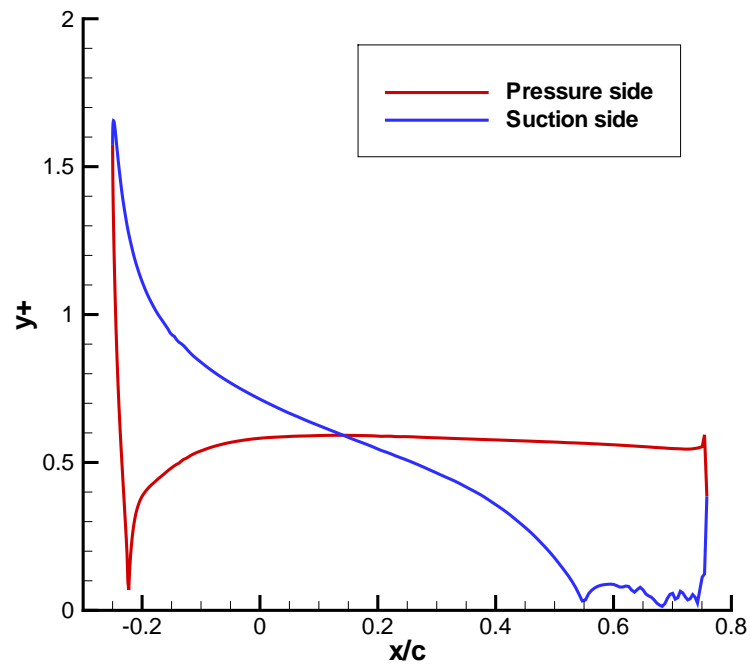


Figure 3.21: Y^+ Distribution over NACA0015 Airfoil

Table 3.11: Computational Details of Spalart-Allmaras and DES Turbulent Model for Turbulent Flow over NACA0015 Airfoil

Model	# of processors	Cpu time (Minute)	Memory requirement (MB)	# of iteration
SA	8	72	76.8	65000
DES	8	87	76.8	65000

Table 3.11 shows the computational details of Set2d DES and Spalart-Allmaras turbulence models. Although both models need equal memory requirement, Spalart-Allmaras is 15 minutes faster than DES.

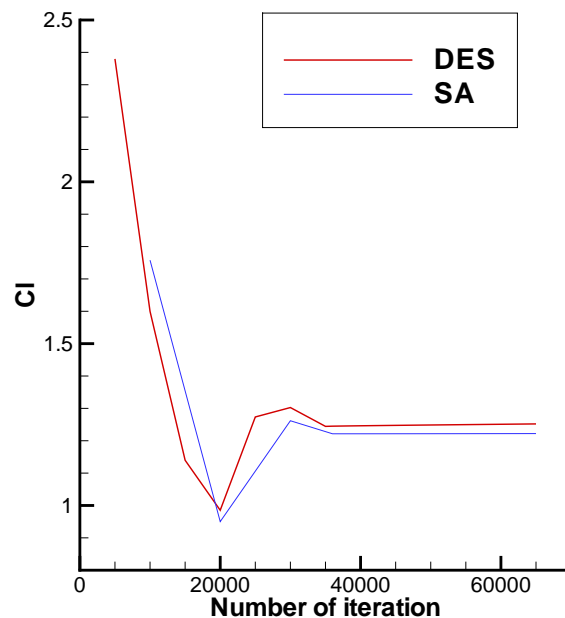


Figure 3.22: Converge History of Lift Coefficient for NACA0015 Airfoil

Figure 3.22 shows the lift convergence histories. Obtained C_L and C_D coefficients are compared with the experimental data [51] and numerical result of Tu et al. [34] and the results of Fluent solver with aid of Table 3.12. It is clearly seen that Set2d and Fluent first order accurate solutions give the C_L and C_D coefficients higher than the experimental data. Both in Set2d and Fluent solvers the DES turbulence model gives higher lift and drag coefficient when compared with Spalart-Allmaras turbulence model. Since numerical result of Tu et al. agree

Table 3.12: Aerodynamic Coefficients for NACA 0015 Airfoil

Model	C_L	C_D
Set2d-DES	1.252	0.074
Set2d-SA	1.222	0.072
Fluent-DES	1.284	0.065
Fluent-SA	1.274	0.058
DES Tu et al. [34]	1.075	0.02
Exp [51]	1.1319	0.01735

well with experimental data, it is seen that high order solutions is needed for calculation of aerodynamic forces in turbulent flows.

As it can be seen in Figure 3.23, after 65000 iterations while Spalart-Allmaras turbulence model converges to 6 order magnitude drop in density residual and 4.4 order magnitude drop in turbulent viscosity, DES turbulence model converges to 5.4 order magnitude drop in density residual and 3.8 order magnitude drop in turbulent viscosity.

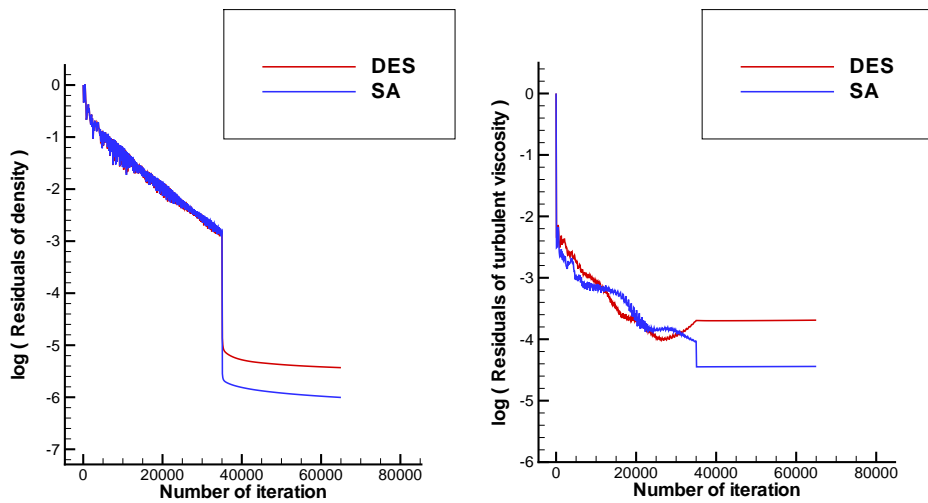


Figure 3.23: Converge History of Residues for NACA0015 Airfoil

The pressure coefficient distribution over the NACA 0015 airfoil is given in Figure 3.24. The obtained results of present solver for DES and Spalart-Allmaras turbulence model show good agreement with each others.

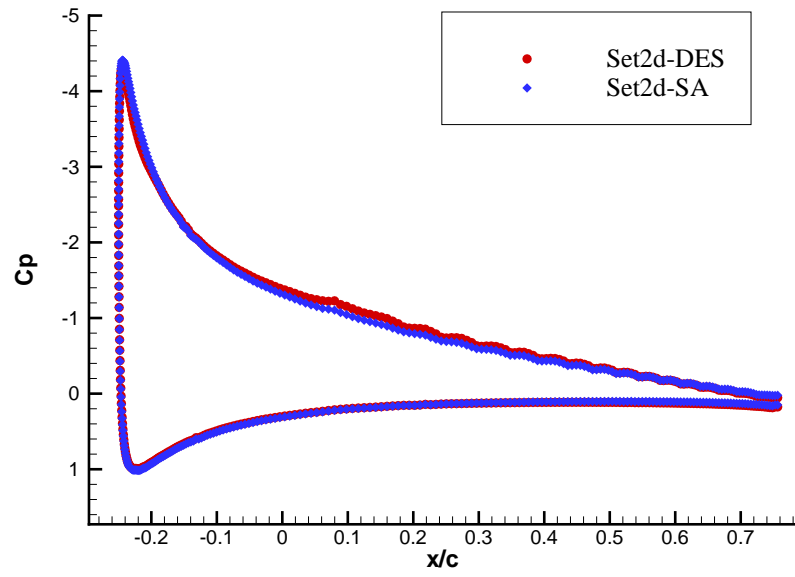


Figure 3.24: Pressure Coefficient Distrubition over NACA 0015 Airfoil for Spalart-Allmaras turbulent model

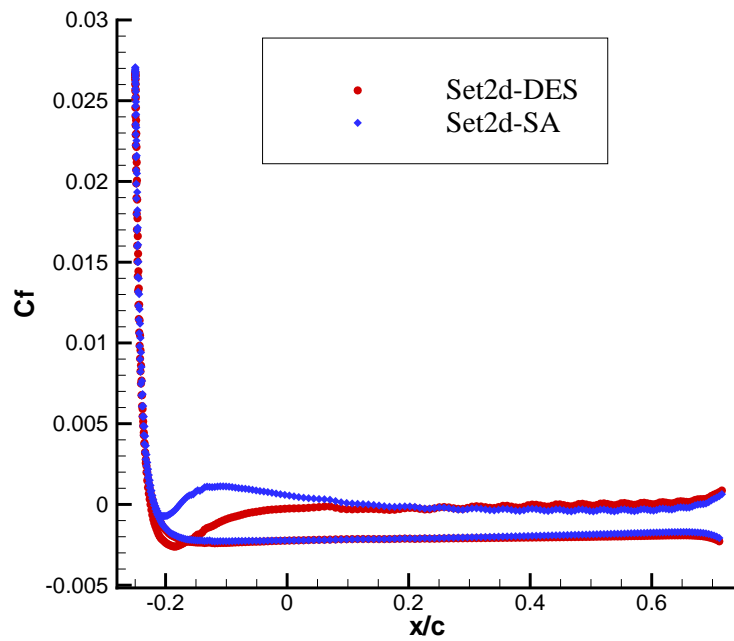


Figure 3.25: Skin Friction Coefficient Distrubition NACA 0015 Airfoil for Spalart-Allmaras turbulent model

Obtained skin friction distribution over airfoil is given in Figure 3.25. When the results compared with each others, it is seen that Set2d-SA gives higher skin friction near leading edge of the upper side of the airfoil. In general, reasonable agreement is seen in skin friction distribution. The Mach number and turbulent viscosity ratio fields of the flow over NACA0015 are

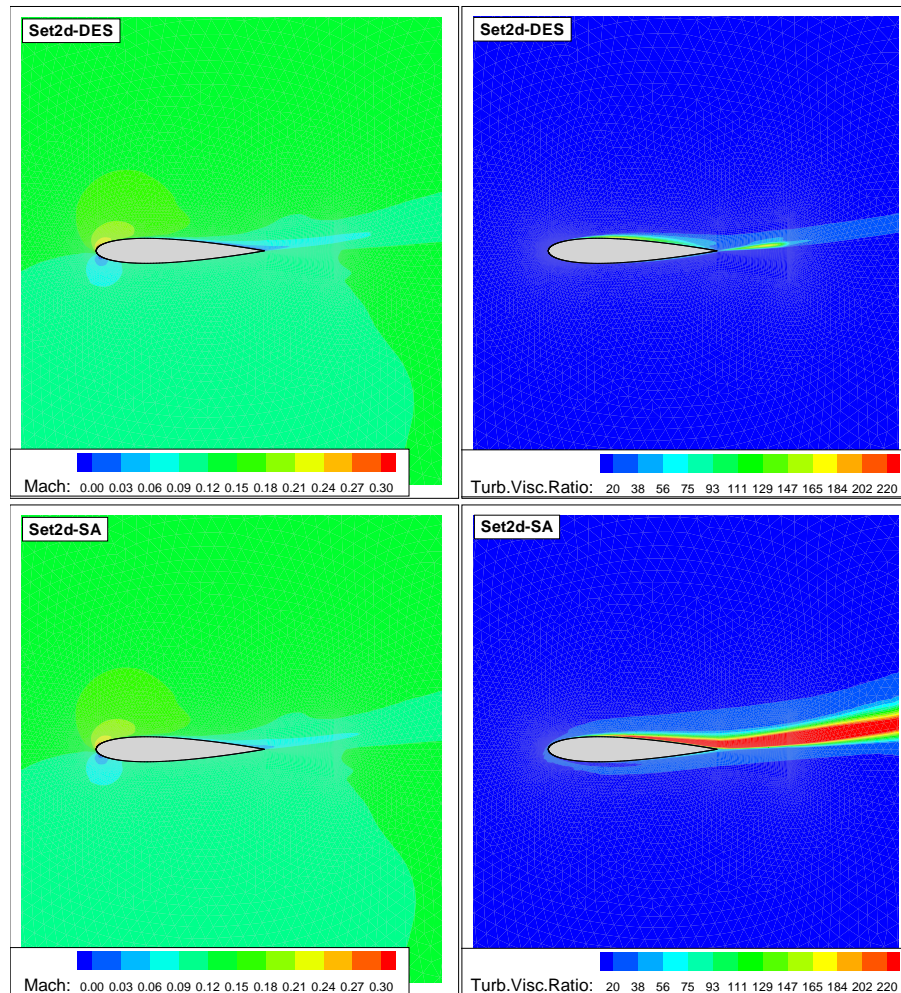


Figure 3.26: Mach Number and Turbulent Viscosity Ratio Contours for NACA 0015 Airfoil given in Figure 3.26. Set2d-DES and Set2d-SA are compared with each other. While Mach number fields of Set2d-DES and Set2d-SA solutions agree well with each other, turbulent viscosity ratio fields of Set2d-DES and Set2d-SA solutions are not similar. Set2d-DES turbulence model produces less turbulence than Set2d-SA turbulence model. This is the expected outcome since DES turbulence model uses different length scale away from the airfoil.

3.4.1 DES Turbulence Model Solution

The pressure coefficient distribution over the NACA 0015 airfoil is given in Figure 3.27. The obtained results of present solver is quite successful at the pressure side of the airfoil. Nevertheless at the suction side non-physical oscillations are observed in DES turbulence model. The creation of very small cells lead to this problem in Finite Volume method. To overcome this problem artificial viscosity ,von Albada flux limiter [50], is needed near regions where strong gradients are take place. Fluent-DES agrees well with Tu et al. since Fluent solves the inviscid fluxes by means of second order accurately Bounded Central-Differencing method.

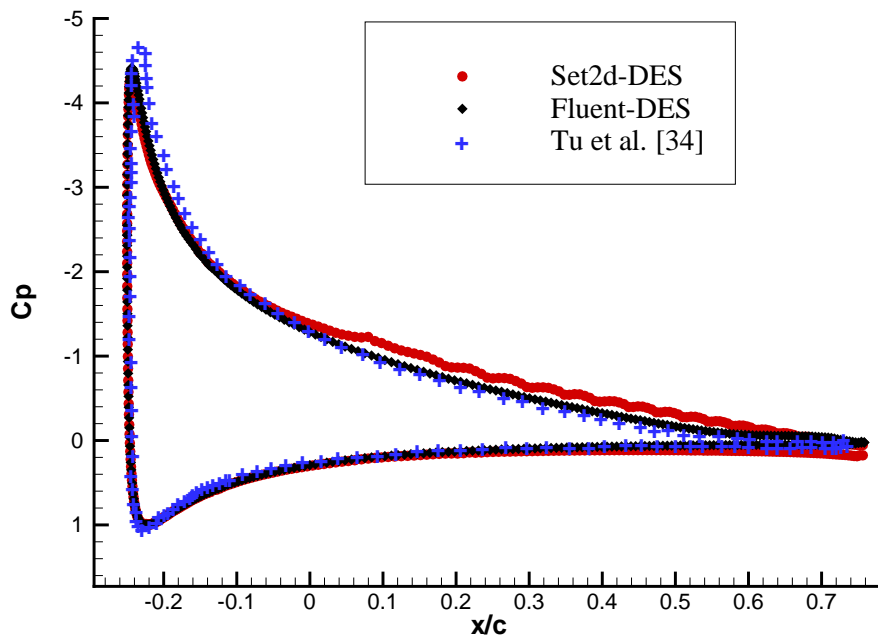


Figure 3.27: Pressure Coefficient Distribution over NACA 0015 Airfoil for DES turbulent model

Obtained skin friction distribution over airfoil is given in Figure 3.28 . When the results compared to Fluent and numerical result of Tu et al., it is seen that Set2d-DES do not show reasonable agreement. This failure attributes to the first order accuracy solutions. First order accurate solutions fail to calculate velocity gradients correctly.

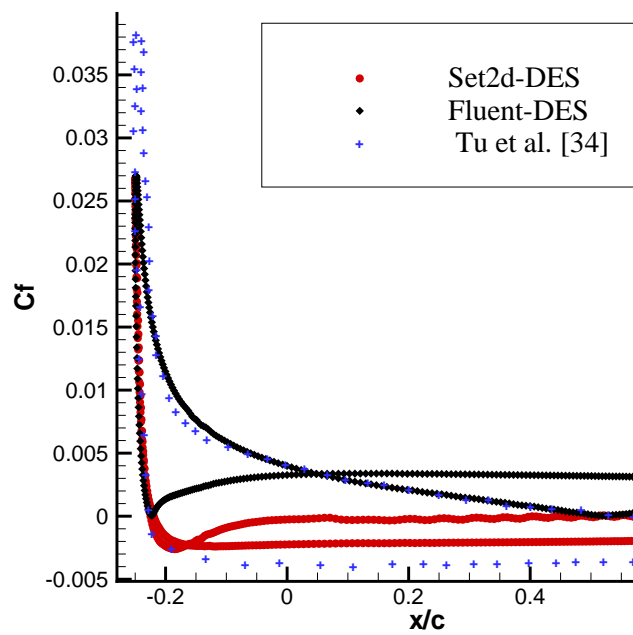


Figure 3.28: Skin Friction Coefficient Distribution NACA 0015 Airfoil for DES turbulent model

CHAPTER 4

CONCLUSIONS

In this thesis, Spalart-Allmaras and DES turbulence models are implemented to the parallel Navier-Stokes solver, Set2d. The Navier-Stokes equations are discretized by cell centered Finite Volume method and solved explicitly by using Runge Kutta time stepping method. Inviscid fluxes are computed by using Roe differencing method. The numerical solution is implemented in parallel environment using domain decomposition algorithm with PVM library routines for inter process communications.

Firstly, DES turbulence model is investigated against the AGARD experimental data for transonic RAE2822 airfoil in steady state flow. It is seen that while grid resolution has a significant effect on the solutions, different y^+ values do not have an important impact and $y^+ \leq 1$ value is enough to obtain turbulent flow solutions with DES turbulence model. If the nature of the used grid is not appropriate to DES turbulence model, Modeled Stress Depletion is observed. In this situation Spalart-Allmaras turbulence model gives better result than DES.

Secondly, flow solutions in subsonic flows for Set2d-DES, Set2d-SA, Fluent-DES and Fluent-SA turbulence models are compared against experimental data and other numerical computations. It is seen that pressure coefficient distributions agree well but two dimensional simulations fail to calculate the skin friction coefficient correctly. The solution of Mach number and turbulent viscosity ratio flow fields are compared with Fluent and Set2d solver. Despite the fact that Mach number contours agree well, it is observed that DES turbulence model underpredicts the turbulent viscosity ratio when compared with Spalart-Allmaras turbulence model.

In conclusion, DES and Spalart-Allmaras turbulence models are implemented successfully to

the Set2d Navier-Stokes solver. They almost produce same turbulence behaviour. First order accurate Set2d solver is not capable of calculating skin friction distributions over airfoils in low subsonic, turbulent flows.

4.1 FUTURE RECOMMENDATIONS

Higher order accuracy methods are needed to investigate turbulence phenomenon since first order accuracy is insufficient in calculating skin friction.

DES solutions at massively separated flows is needed to assessed in Set2d solver.

DES turbulence model is too sensitive to the grids and this cause Modeled Stress Depletion. Delayed Detached Eddy Simulation (DDES) can be implemented instead of standard DES.

Optimization of the code is needed to construct more efficient algorithm for reducing overall computational cost.

REFERENCES

- [1] Carl, H. Gibson “*Turbulence in the Ocean, Atmosphere, Galaxy, and Universe*”, Appl. Mech. Rev. 49, no. 5, 299-315, May 1996
- [2] McDonough, J.M. “*Introductory Lectures on Turbulence Physics, Mathematics and Modeling*”, Departments of Mechanical Engineering and Mathematics university of Kentucky, 2007
- [3] Paul E. Dimotakis, Richard C. Miake-Lye, and Dimitris A. Papantoniou, “*Structure and Dynamics of Round Turbulent Jets*”, Phys. Fluids 26,3185(1983), doi:10.1063/1.864090
- [4] Aybay Orhan, “*Time-Conservative Finite-Volume Method with Large-Eddy Simulation for Computational Aeroacoustics*”, Doctoral thesis, Durham University, 2010.
- [5] Anderson, J.D. “*Computational Fluid Dynamics: The Basics with Applications*”, Int. Ed., McGraw-Hill Singapore, 1995.
- [6] Çıray Cahit “*A Critical View on Closure or What is the Big Problem of Turbulence?*”, 6th Ankara International Aerospace Conference, 2011.
- [7] Hoffman K.A., Chiang S.T. “*Computational Fluid Dynamics*”, Volume-3, Engineering Education System Publication, USA, August 2000.
- [8] Wilcox David C. “*Turbulence Modeling for CFD*”, Second printing, DCW industries, USA, 1994.
- [9] Pope Stephen B., “*Turbulent Flows*”, Cambridge University Press, 2000.
- [10] Girimaji, S.S. “*Partially-Averaged Navier-Stokes Method for Turbulence: A Reynolds-Averaged Navier-Stokes to Direct Numerical Simulation Bridging Method*”, Journal of Applied Mechanics, 73, 413-421, 2006.
- [11] “<http://www.mech.kth.se/stefanw/AppliedCFD/02-Turbulence.pdf>”, SG2224, Applied Computational Fluid Dynamics course website last visited on 15-11-11.
- [12] Aybay Orhan, “*Implementation of the Spalart-Allmaras Turbulence Model to a Two-Dimensional Unstructured Navier-Stokes Solver*”, M.S Thesis, METU, 2004.
- [13] Spalart, P.R. and Allmaras, S.R., “*A One-Equation Turbulence Model for Aerodynamics Flows*”, Boeing Commercial Airplane Group, Seattle, Washington, 1992.
- [14] Paciorri R., Dieudonne W., Degrez G., Charbonnier J.M., Deconinck H., “*Validation of the Spalart-Allmaras Turbulence Model for Application in Hypersonic Flows*”, von Karman Institute for Fluid Dynamics, Saint-Genesius-Rode, Belgium, AIAA, 1997.
- [15] NASA website “<http://turbmodels.larc.nasa.gov/spalart.html>”, last visited on 15-11-11.

- [16] Travin A, Shur M, Strelets M, Spalart PR. “*Detached-Eddy Simulations Past a Circular Cylinder*”, Flow Turbul. Combust. 63:293-313
- [17] Shur M, Spalart P.R., Strelets M., Travin A. “*Detached-Eddy Simulations of an Airfoil at High Angle of Attack*”, Engineering Turbulence Modelling and Experiments, Vol. 4, pp.669-678, 1999
- [18] Spalart PR. “*Young Person’s Guide to Detached-Eddy Simulation Grids*”, Tech. Rep. NASA CR-2001-211032, July, 2001
- [19] Radoslav Bozinoski, Roger L. Davis, “*A DES Procedure Applied to the Flow over a NACA0012 Airfoil*”, International Review of Aerospace Engineering, April, 2010
- [20] Benezza A., Blanco E., Abidat M., “*2D Detached-Eddy Simulation Around Elliptic Airfoil at High Reynolds Number*”, Journal of Applied Sciences, pp.547-552, 2007
- [21] Kunz F.R., Lindau J.W., Kaday T.A., Peltier L.J., “*Unsteady RANS and Detached Eddy Simulation of Cavitating Flow Over a Hydrofil*”, Fifth International Symposium on Cavitation, Osaka, Japan, November, 2003
- [22] Lopez O.D., Moser R.D, “*Delayed Detached Eddy Simulation of Flow Over an Airfoil with Synthetic Jet Control*”, Mecanica Computacional, Vol XXVII, pp3225-3245, 2008
- [23] Spalart P.R., Deck S., Shur M.L., Squires K.D., Strelets M.Kh., Travin A, “*A New Version of Detached-Eddy Simulation, Resistant to Ambiguous Grid Densities*”, Theor. Comput Fluid Dyn, 2006
- [24] Deck Sebastien, “*Zonal-Detached-Eddy Simulation of the Flow Around a High-Lift Configuration*”, AIAA Journal, Vol.43, No.11, November, 2005
- [25] Spalart PR. “*Detached-Eddy Simulation*”, Annual Review of Fluid Mechanics, 2009
- [26] Travin A., Shur M., Strelets M., Spalart P.R., “*Detached-Eddy Simulations Past a Circular Cylinder*”, Flow, Turbulence and Combustion, 63: 293-313, 2000
- [27] Frana K., Honzejk V., “*A Comparison Between Classical DES and DDES Using the In-House Computational Code*”, Selected Topics in System Science and Simulation in Engineering, ISBN: 978-960-474-230-1
- [28] Panguluri Sri S., “*Implementation and Validation of the Hybrid Turbulence Models in an Unstructured Grid Code*”, Msc. Thesis, Kentucky University, 2007
- [29] Mockett Charles “*A Comprehensive Study of Detached-Eddy Simulation*”, Phd. Thesis, Berlin Institute of Technology, 2009
- [30] FLOMANIA PROJECT website “<http://cfd.mace.manchester.ac.uk/flomania/index2.html>”, last visited on 15-04-12.
- [31] DESider PROJECT website “<http://cfd.mace.manchester.ac.uk/desider/index2.html>”, last visited on 15-04-12.
- [32] Haase W., Aupoix B., Bunge U., Schwaborn D., “*FLOMANIA - A European Initiative on Flow Physics Modelling*”, Notes on Numerical Fluid Mechanics and Multidisciplinary Design, Vol.94, 2006

- [33] Haase W, Braza M., Revell A., “*DESider - A European Effort on Hybrid RANS-LES Modelling*”, Notes on Numerical Fluid Mechanics and Multidisciplinary Design, Vol.103, 2009
- [34] Tu S.,Aliabadi S.,Patel R.,Watts M., “*An Implementation of the Spalart-Allmaras DES Model in an Implicit Unstructured Hybrid Finite Volume/Element Solver for Incompressible Turbulent Flow*”, International Journal For Numerical Methods In Fluids, 59: 1051-1062, 2009.
- [35] Davidson Lars, “*LESFOIL: A European Project on Large Eddy Simulations Around a High-Lift Airfoil at High Reynolds Number*”, ECCOMAS, Barcelona, 2000.
- [36] Schmidt S., Thiele F., “*Detached Eddy Simulation of Flow Around A-Airfoil*”, Flow, Turbulence and Combustion 71: 261-278, 2003.
- [37] Breuer M.,Jovicic N., Mazaev K., “*Comparison of DES, RANS and LES for the Separated Flow Around a Flat Plate at High Incidence*”, International Journal For Numerical Methods In Fluids, 41: 357-388, 2003.
- [38] Gilling L., Sorensen N.N., Davidson L., “*Detached Eddy Simulation of an Airfoil in Turbulent Inflow*”, 47th AIAA Aerospace Sciences Meeting Including The New Horizons Forum and Aerospace Exposition, Orlando, Florida, January, 2009.
- [39] Dong Li, “*Numerical Simulation of Thin Airfoil Stall by Using a Modified DES Approach*”, International Journal For Numerical Methods In Fluids, 54: 325-332, 2007.
- [40] Madsen J., Lenz K., Dynampally P, Sudhakar P., “*Investigation of Grid Resolution Requirement for Detached Eddy Simulation of Flow Around Thick Airfoils Sections*”, Europe’s Premier Wind Energy Event, Marseille, 2009.
- [41] Kotapati-Apparao R.B., Squires K.D., Forsythe J.R., “*Prediction of the Flow Over an Airfoil at Maximum Lift*”, AIAA,2004.
- [42] Cokljat D., Liu F., “*DES of Turbulent Flow Over an Airfoil at High Incidences*”, Fluent Technical Notes TN170, 2002.
- [43] Vivek Krishnan, “*Advanced Detached Eddy Simulation*”, Phd. Thesis, Arizona State University, August, 2008
- [44] Jameson A., Schmidt D. and Turkel E., “*Numerical Solutions of the Euler Equations by Finite Volume Method Using Runge-Kutta Time-Stepping Schemes*”, AIAA 14th Fluid and Plasma Dynamics Conference, AIAA-81-1259, June 1981.
- [45] Lin C-W, Percival S, Gotimer E.H. “*Viscous Drag Calculations for Ship Hull Geometry*”, The 9th International Conference on Numerical Methods in Laminar and Turbulent Flow, Atlanta, GA, 1995.
- [46] Thibert, J.J., Grandjacques, M. and Ohman, L.H., “*Experimental Data Base for Computer Program Assesment*”, AGARD, AR-138, May, 1979.
- [47] Chit Ong J., Omar Ashraf A. and Asrar Waqar, “*Reynolds Averaged Navier Stokes Flow Computation of Rae2822 Airfoil Using Gas-kinetic BGK Scheme*”, Proceedings of the International Multiconference of Engineers and Computer Scientists, Vol. II, 2009, IMECS 2009, Hong Kong.

- [48] W. Haase, E. Chaput et al., “*Validation of CFD Codes and Assessment of Turbulence Models*”, European Computational Aerodynamics Research Project, Notes on Numerical Fluid Mechanics, Vol 58, pp. 327-346, 1996
- [49] Roe A. Robert “*World Directory of Aerospace Research and Development*”, GAO/NSIAD-90-71FS Foreign Test Facilities, June 22, 1990
- [50] “http://en.wikipedia.org/wiki/Flux_limiter”, site last visited on 01-09-12.
- [51] Sheldahl Robert E., Klimas Paul C. “*Aerodynamic Characteristics of Seven Symmetrical Airfoil Sections Through 180-Degree Angle of Attack for Use in Aerodynamic Analysis of Vertical Axis Wind Turbines*”, Sandia National Laboratories, Report SAND80-2114, 1981.

Appendix A

Non-Dimensionalization of Governing Equations

In CFD non-dimensionalization of the conservative quantities gets rid of the requirement of converting from one system to another within the code.

The flow variables in the governing equations are non-dimensionalized with the free stream values of density, ρ_∞ , speed of sound, a_∞ , dynamic viscosity, μ_∞ , and reference length L . The non-dimensional flow variables can be seen in table A.1.

$\rho = \frac{\rho^*}{\rho_\infty}$	$x = \frac{x^*}{L}$	$y = \frac{y^*}{L}$	$a = \frac{a^*}{a_\infty}$
$e = \frac{e^*}{a_\infty}$	$u = \frac{u^*}{a_\infty}$	$v = \frac{v^*}{a_\infty}$	$p = \frac{p^*}{\rho_\infty a_\infty^2}$
$\mu = \frac{\mu^*}{\mu_\infty}$	$t = \frac{t^* a_\infty}{L}$	$T = \frac{T^*}{T_\infty}$	$\mu_t = \frac{\mu_t^*}{\mu_\infty}$

Table A.1: Non-dimensional Variables.

$$\begin{array}{lll} \rho_\infty = 1 & L = \text{chordlength} & p_\infty = \frac{1}{\gamma} \\ a_\infty = 1 & T_\infty = 1 & \mu_\infty = 1 \end{array}$$

Appendix B

Sample Input Data

0.3	Inflow Mach Number
2.0E6	Reynolds Number
0.0	Angle of Attack (degree)
121	Isolve (n1: n2:n3)
0.8	CFL number
500	# of time step to run
20	Output frequency of residual
8	Npar, # of partitions
10	Anutin for initialization
100	Output frequency of solutions

isolve :

- n1 = 1 : Explicit solution
- n2 = 0 : Inviscid solution
- n2 = 1 : Viscous, laminar flow solution
- n2 = 2 : Turbulent flow solution with Spalart-Allmaras based DES model
- n3 = 1 : Roe flux difference splitting
- n3 = 2 : HLLC flux difference splitting
- n3 = 3 : ZhaBilgen
- n3 = 4 : AUSM
- n3 = 5 : VanLeer
- n3 = 6 : Upwind flux

Appendix C

Mesh File Format

```
20418 (node #) 26768 (cell #)
x y
0.292280000000E-01 0.213480000000E-01
0.292280000000E-01 -0.217220000000E-01
0.239545068731E-01 0.193976376547E-01
0.196318064299E-01 0.176460428881E-01
0.160627341725E-01 0.160191268907E-01
0.130831932370E-01 0.145040525049E-01
0.105741111849E-01 0.130777709580E-01
0.844501352241E-02 0.117183395373E-01
. .
. .
. .
. .
n1 n2 n3 n4 neigh1 neigh2 neigh3 neigh4 (connectivity and neighbouring)
14698 18446 14697 22611 22620 -1
18412 18430 18446 22565 22614 322611
398 1000 120 34 2710 2754 -2 5395
37 869 3625 463 16455 2797 2836 5410
. .
. .
```